



THE UNIVERSITY OF QUEENSLAND  
A U S T R A L I A

**A Theoretical Study of Graphene Oxide Chemical Structure**

Haining Luo

Bachelor of Materials Engineering

*A thesis submitted for the degree of Master of Philosophy at*

*The University of Queensland in 2017*

The School of Mechanical and Mining Engineering

## **Abstract**

Graphene is a 2D material that has many unique and excellent physical and electrical properties. Since its discovery, people have spent much time and money on the research of graphene. A film of graphene is transparent, conductive, flexible, light in weight but very strong. Unfortunately, research in the last decade has proved that it is nearly impossible to fabricate stable, defect-free, large scale graphene sheets which have extensive application, yet without any commercial success. However, compared with the high cost of graphene film, graphene oxide (GO) is an easy-to-make material which has a similar structure. The obstacle for GO's application is its low reproducibility since a number of oxidized side chains are difficult to remove. Even today, the GO structure model is still controversial.

This study introduces a new structural model of graphene oxide and its theoretical electronic properties. A number of different models for graphene oxide have been proposed and tested using ab initio calculations. The main simulation and computation theories to establish these structure models in this study are molecular mechanics (MM) and density functional theory (DFT). In the proposed GO structure, the para-substituted epoxide groups stay in close proximity to, but on the opposite sides of the carbon plane, to the hydroxyl molecule. On the edge of GO sheet, the carboxyl prefers attachment in the armchair orientation, while the carbonyl prefers the zigzag orientation. The carbon backbone has a moderate wrinkling located around hydroxyl and epoxide molecules but still maintains a hexagonal graphene-like structure. This configuration repeats along the carbon network with subtle variations so that the chemical composition of GO is variable from  $C_{1.5}O$  to  $C_{2.5}O$ . And the electronic model also suggests that the band gap of GO can be theoretically tuned both by chemical reduction and controlled oxidation process.

**Declaration by author**

This thesis is composed of my original work, and contains no material previously published or written by another person except where due reference has been made in the text. I have clearly stated the contribution by others to jointly-authored works that I have included in my thesis.

I have clearly stated the contribution of others to my thesis as a whole, including statistical assistance, survey design, data analysis, significant technical procedures, professional editorial advice, and any other original research work used or reported in my thesis. The content of my thesis is the result of work I have carried out since the commencement of my research higher degree candidature and does not include a substantial part of work that has been submitted to qualify for the award of any other degree or diploma in any university or other tertiary institution. I have clearly stated which parts of my thesis, if any, have been submitted to qualify for another award.

I acknowledge that an electronic copy of my thesis must be lodged with the University Library and, subject to the policy and procedures of The University of Queensland, the thesis be made available for research and study in accordance with the Copyright Act 1968 unless a period of embargo has been approved by the Dean of the Graduate School.

I acknowledge that copyright of all material contained in my thesis resides with the copyright holder(s) of that material. Where appropriate I have obtained copyright permission from the copyright holder to reproduce material in this thesis.

### **Publications during candidature**

Poster: *The Theoretical Study of Graphene Oxide* on the 24th Australian Conference on Microscopy and Microanalysis 2016.

### **Publications included in this thesis**

No publications included.

**Contributions by others to the thesis**

Dr Graeme Auchterlonie and Prof Jin Zou have contributed to propose of the research concept and also critically revising the thesis.

**Statement of parts of the thesis submitted to qualify for the award of another degree**

None

## **Acknowledgements**

I would like to thank my supervisors, Professor Jin Zou and Doctor Graeme Auchterlonie, for offering me an opportunity to do research in graphene oxide modelling. They have shown great patience throughout the last 2 years guiding me on the right path of research. I truly appreciate their support and advice on my project.

Also, I would like to thank my fellows in Prof Jin's research group: Yichao Zou, Lei Yang, Min Hong, Chen Zhou, Liqing Huang, Van Nguyen, Han Gao, Raza Moshwan, Xiaolei Shi, Weidi Liu, Shijian Liu, Qiang SUN, Shijian Liu, Qizhen Li, Yuan Wang. They all encourage and help me a lot when I met difficulties in my study.

This work was supported by Australian Research Council. The Research Computing Centre at the University of Queensland and the National eResearch Collaboration Tools and Resources (Nectar) project were also acknowledged.

**Keywords**

KEYWORDS: graphene oxide, structural model, thermodynamics, molecular mechanics, density functional theory, band gap

**Australian and New Zealand Standard Research Classifications (ANZSRC)**

ANZSRC code: 091299 Materials Engineering not elsewhere classified, 100%

**Fields of Research (FoR) Classification**

FoR code: 0912 Materials Engineering, 100%

# Contents

Chapter 1. Introduction.....	12
1.1 Introduction .....	12
1.2 Outline .....	12
Chapter 2. Literature Review.....	14
2.1 Graphene .....	14
2.1.1 Structure .....	14
2.1.2 Electrical Properties .....	14
2.1.3 Synthesis method .....	15
2.2 Graphene Oxide.....	17
2.2.1 Characterizations.....	18
2.2.2 Chemical structure .....	21
Chapter 3. Computational Methods.....	24
Chapter 4. Results and discussion .....	26
4.1 Determination of Thermodynamically Stable Structures.....	26
4.2 Interaction of Functional Groups .....	29
4.3 Electronic Properties .....	31
Chapter 5. Summary and Future Work.....	34
5.1 Summary .....	34
5.2 Future Work .....	35
References.....	37
Appendix 1 .....	43
Appendix 2.....	44



# Table of Figures

Figure 2.1 (a) Unit cell of graphene including two non-equivalent atom positions A and B; (b) two types of edges in graphene flake: Zigzag and armchair. ....	14
Figure 2.2 Schematic First Brillouin zone and band structure of graphene. The Dirac points K and K' are the transition between the conduction band and the valence band.[16] .....	15
Figure 2.3 Comparison of the graphene production methods. The methods were evaluated in five terms: graphene quality (G), yield (Y), purity (P), scalability (S) and cost efficiency (C) of the whole production process. The figure was adapted from ref [17]. ....	16
Figure 2.4 The diagram illustrates the CVD steps of graphene growth on copper: (a) Surface oxide on copper foil; (b) the nucleation of graphene in CH <sub>4</sub> /H <sub>2</sub> atmosphere at 1000 C; (c) oriented growth of the graphene flakes. The figure was adapted from [27] .....	17
Figure 2.5 Schematic of the roll to roll method. The production process includes: adhesion of polymer supports, copper etching and dry transfer-printing on a target substrate. The figure was adapted from ref [28]. ....	17
Figure 2.6 (A) 1D <sup>13</sup> C MAS and (B) 2D <sup>13</sup> C/ <sup>13</sup> C chemical-shift correlation solid-state NMR spectra of <sup>13</sup> C-labeled graphite oxide with (C) slices selected from the 2D spectrum at the indicated positions (70, 101, 130, 169, and 193 ppm) in the w1 dimension. This figure was adapted from ref [32]. ....	18
Figure 2.7 (a) FTIR spectrum of GO; (b) UV-vis spectrum (c) Raman spectrum [1] .....	19
Figure 2.8 (a) XRD spectrum of graphene oxide (GO) and graphene (GR); (b) XPS spectrum of GO and GR. [37] .....	20
Figure 2.9 (a) TEM image of a single GO sheet on a carbon support. (b) Labelled SAED of the GO sheet in a. (c) Intensity profile through the diffraction spots labelled in panel b. (d) Contact-mode AFM scan of reduced graphene oxide etched on a graphene oxide paper substrate (e) Height profile through the dashed line shown in (d) The figure was adapted from ref [2] .....	20
Figure 2.10 (a) Hofmann model; (b) Ruess model ; (c) Scholz-Boehm model ; (d) Nakajima-Matsuo model ; (e) Lerf-Klinowski model; (f) Dekany model [42] .....	21
Figure 4.2 C <sub>60</sub> 4 models and MM steric energies. ....	27
Figure 4.3 C <sub>240</sub> 16 and C <sub>540</sub> 36 models steric energies. ....	27
Figure 4.4 Tension caused by sp <sup>3</sup> hybridization between α-C and β-C (red arrows); two carbon positions: α-C, directly bonded to oxygen; β-C, three atoms bonded to α-C. ....	28
Table 1 GO edge model and MM steric energies .....	28

Figure 4.5	Supercells of: a) 1, 4-trans-epoxy structure; b) chainlike structure. The grey, red and white spheres represent carbon, oxygen and hydrogen atoms respectively. The determined $E_b$ is shown at the top. ....	30
Figure 4.6	a) H-bonds (blue dashed lines) sketch in GO; b) Charge density map of the b-type GO model. ....	30
Figure 4.7	Supercells of a), b) Cis-configuration GO model with two epoxy groups; c), d) Trans-configuration GO model with two epoxy groups. The total energy is shown above the side-view model. ....	31
Figure 4.8	Band structures of pristine graphene a) and GO with b) a single hydroxyl, and c) a single epoxy. All using a $2 \times 2$ supercell. ....	32
Figure 4.9	Density of states of a) hydroxyl chainlike structure; b) 1, 4-trans-epoxy structure c) 1, 4-trans-epoxy structure with pure graphene stripe area. ....	33
Figure 4.10	New Proposed thermodynamic GO structure model of GO. The grey, red and white spheres represent carbon, oxygen and hydrogen atoms respectively. The yellow areas represent pure graphene regions and the blue dashed lines represent the hydrogen bond networks. ....	34

# List of Abbreviations used in the thesis

**2-D:** Two Dimensional

**CVD:** Chemical Vapour Deposition

**GO:** Graphene Oxide

**DFT:** Density Functional Theory

**FPLAPW + lo:** Full Potential Linear Augmented Plane Wave plus Local Orbitals

**PECVD:** Plasma Enhanced Chemical Vapour Deposition

**SSNMR:** Solid State Nuclear Magnetic Resonance

**FTIR:** Fourier Transform Infrared Spectroscopy

**DRIFT:** Diffuse Reflectance Mode Fourier Transform Infrared Spectroscopy

**UV-vis:** Ultraviolet–visible Spectroscopy

**XRD:** X-ray Diffraction Spectroscopy

**XPS:** X-ray photoelectron spectroscopy

**TEM:** Transmission Electron Microscopy

**AFM:** Atomic Force Microscopy

**TGA:** Thermal Gravimetric Analysis

**LK Model:** Lerf-Klinowski Model

**MD:** Molecular Dynamics

**MM:** Molecular Mechanics

**GEDIIIS:** Energy-represented Direct Inversion in the Iterative Subspace for Geometry Optimization

**PBE:** Perdew–Burke–Ernzerhof

**SCF:** Self-Consistent Field

**FP-LAPW:** Full Potential Linear Augmented Plane Wave

**GGA:** Generalized Gradient Approximation

**H-bond:** Hydrogen Bond

**ITO:** Indium Tin Oxide

# Chapter 1. INTRODUCTION

## 1.1 INTRODUCTION

In 2004, the first graphene film was isolated from graphite in the laboratory by Andre Geim and Kostya Novoselov [3]. Graphene is a 2-D material with a hexagonal structure [3]. The single layer graphene has many peculiar electrical, mechanical and optical properties [4]. High electrical conductivity and high optical transmittance are two major advantages for graphene to be used as transparent conductor [4, 5]. But till today, the extraordinary performance only exists in laboratory. One of the most critical obstacles is that there is still no method to prepare large-scale and low-defect graphene films [6-8].

Graphene oxide (GO), as one of the source materials for synthesis of graphene, has been studied in recent years. Not only the large scale graphene production can be achieved by reduction of GO with a relatively low cost, but also the GO itself has many potential applications in batteries and transparent conductors. A precise GO structural model can help us understand the electronic, mechanical and optoelectronic properties of GO. As a result, we can design new GO composites or intentionally tune the properties of GO based on the model.

Although there are many experimental and theoretical models, the real structure of GO still remains controversial. One reason is that these models arrange the oxygen groups manually in a fixed cell within a limited scale, but the real GO may be non-stoichiometric and non-periodic in the long range. As a consequence, in this study, a new thermodynamic GO structure is proposed both in a large scale molecular mechanics (MM) models and a precise DFT model. The MM2 method [9] is one of the most reliable MM methods developed to calculate the properties of organic molecular models in recent modelling studies [10-12]. While DFT is a computational quantum mechanical modelling method used to investigate the chemical and electronic structures (principally the ground state) of many-body systems. Depending upon the synthesis process, highly oxidized GO has different compositions varying from  $C_{1.5}O$  to  $C_{2.5}O$  [13, 14] while the fully oxidized area of GO model in this study has a C/O ratio of 1.5:1.

## 1.2 OUTLINE

The thesis is organized as follow. Chapter 1 is an overview of the research background, the significance of studying GO structural model and the scope of the thesis. The literature review about the current graphene and graphene oxide research will be covered in Chapter 2. The first section of Chapter 2 introduces basic structure, electronic properties and synthesis methods of

graphene. The second section describes both the experimental and theoretical approaches to establish the GO structural model. Chapter 3 is devoted to explain the theory and computational methods used in this study. Chapter 4 discusses the results of molecular mechanics and density functional theory calculations including determination of thermodynamically stable structure, interactions between functional groups and the electronic properties. Chapter 5 summaries the conclusion of this theoretical study and presents the future work.

## Chapter 2. LITERATURE REVIEW AND RESEARCH GAPS

### 2.1 GRAPHENE

#### 2.1.1 Structure

Graphene is a single layer crystal of carbon atoms, usually exfoliated from graphite. It has a honeycomb hexagonal lattice fabricated by  $sp^2$  hybridized bonds. The rhombic unit cell of single layer graphene contains two carbon atoms A and B (Figure 2.1). The C-C distance is 0.142 nm. The graphene crystal is not a perfect 2D plane, but contains ripples around 1 nm in size.

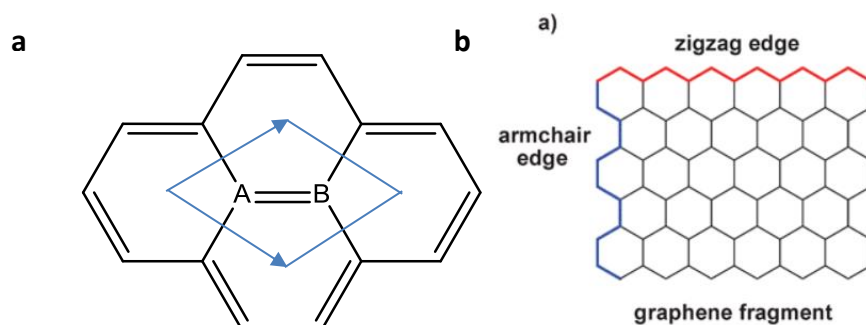


Figure 2.1 (a) Unit cell of graphene including two non-equivalent atom positions A and B; (b) two types of edges in graphene flake: Zigzag and armchair.

The idea graphene is an infinite 2D structure, but what we really studied in laboratory are the graphene flakes with edges. In Figure 2.1 (b), there are two types of edges, notably, armchair and zigzag. These two kinds of edges lead to different electronic properties of graphene flakes.

#### 2.1.2 Electrical Properties

Graphene has been discovered as a zero-gap semiconductor [15]. As shown in Figure 2.2, the valence bands meet the conduction bands at Dirac points and Dirac points locate on the six corners of the Brillouin zone in momentum space[15]. There are two non-equivalent sets of Dirac points labelled K and K'. Due to the linear dispersion near the Dirac points, the charge carriers (holes and electrons) can transform to each other without energy consumption [15]. These charge carriers with low energy can be described as massless Dirac fermions [15]. By changing the applied electric field, the specific carrier density can be changed as well. Another advantage from the presence of Dirac points is the electronic ballistic transport of charge carriers in graphene [15]. Charge carriers in graphene behave like relativistic particles with an effective speed of light given by the Fermi velocity[15]. The ballistic mean free path of graphene charge carriers can be  $0.3\mu\text{m}$  [16]. This behavior attracts much research attention and becomes one of the most intriguing properties of graphene.

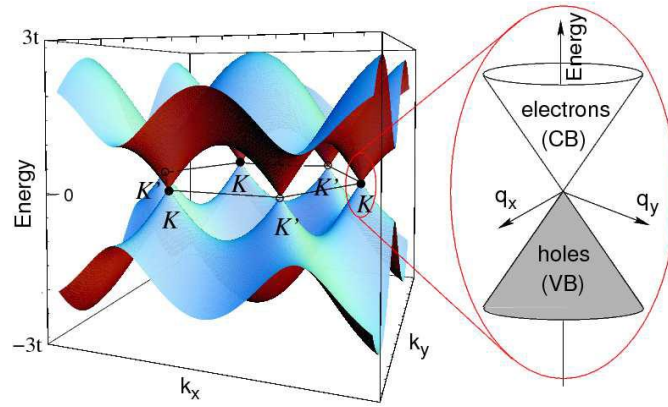


Figure 2.2 Schematic First Brillouin zone and band structure of graphene. The Dirac points  $K$  and  $K'$  are the transition between the conduction band and the valence band.[16]

### 2.1.3 Synthesis method

The first single layer graphene was extracted from highly oriented pyrolytic graphite by Andre Geim and Kostya Novoselov using the scotch tape. Until now, there is no process developed that can make graphene sample with such high carrier mobility and low density of defects [17]. However, mechanical exfoliation is limited in production scale and time consuming. This disadvantage limits the application to fundamental research of graphene.

After more than 10 years' development, for today's industrial production of graphene, there are two major synthesis routes: bottom-up epitaxial growth and top-down exfoliation [4]. The bottom-up epitaxial growth approach involves the direct synthesis of graphene materials from the carbon sources [4]. A typical method, for example, is the chemical vapor deposition (CVD). CVD is usually used to grow large-scale, single or multi-layer graphene sheets on metal substrates with low defects density [4, 8]. Differently, the top-down approaches such as reduction of graphene oxide (GO) take advantages of high yield, ease of implementation, and solution-based process ability [4, 18]. In particular, the low-cost and mass production of reduced graphene oxide sheets has been realized [4, 19]. The Figure 2.3 summarizes the pros and cons of common production methods of graphene.

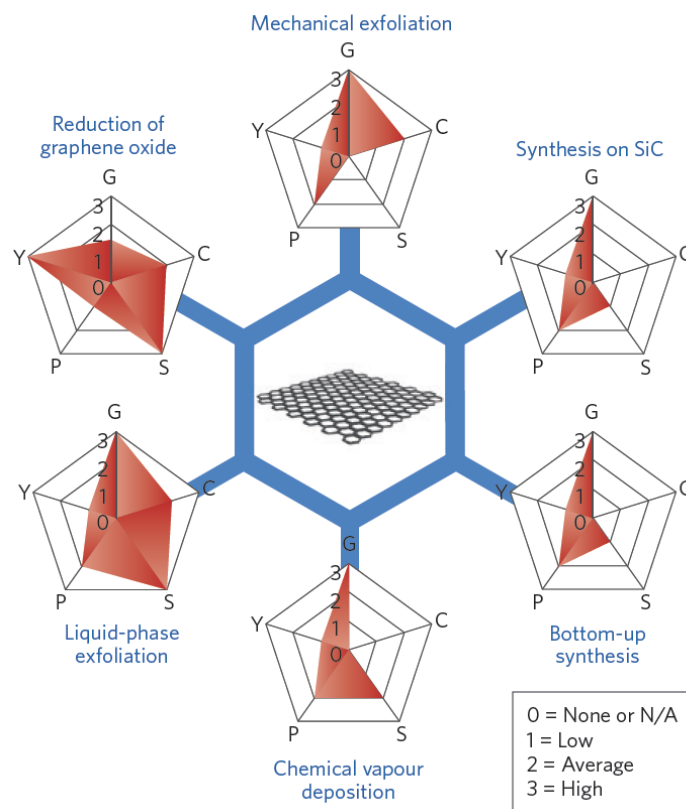


Figure 2.3 Comparison of the graphene production methods. The methods were evaluated in five terms: graphene quality (G), yield (Y), purity (P), scalability (S) and cost efficiency (C) of the whole production process. The figure was adapted from ref [17].

Among these methods, reduction of graphene oxide (GO) was thought to be one of the most prominent methods to achieve the large scale and low-cost production of graphene [19]. GO as a highly oxidized sheet is synthesized from strong oxidation of pristine graphite followed by mechanical exfoliation such as ultra-sonication in liquid media or just stirring [18, 20]. The  $\pi$  network of the graphene contributes to the conductive characteristic of graphene, so the GO must be reduced to recover its  $\pi$  bond [19]. The GO are usually reduced by electrochemical, thermal and chemical processes [19]. The products do not have a very high quality because of the presence of extrinsic defects (oxygen groups) and intrinsic defects (edges and deformations), but this method allows the production with high yield and relatively low costs. Thus, oxidation of graphite, mechanical exfoliation and reduction of GO are the popular methods to produce commercial graphene.

The most popular methods reported recently [21-27] are chemical vapor deposition (CVD) or plasma enhanced chemical vapor deposition (PECVD) which can produce large scale and moderate quality graphene films. The major process of CVD is shown in Figure 2.4.



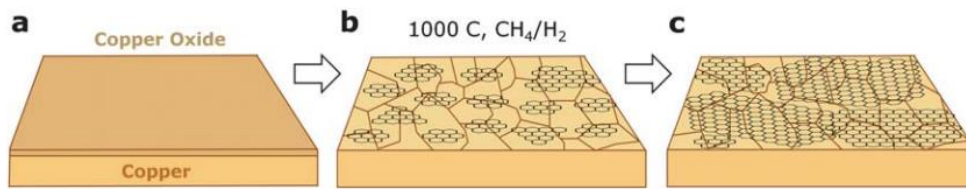


Figure 2.4 The diagram illustrates the CVD steps of graphene growth on copper: (a) Surface oxide on copper foil; (b) the nucleation of graphene in CH<sub>4</sub>/H<sub>2</sub> atmosphere at 1000 C; (c) oriented growth of the graphene flakes. The figure was adapted from [27]

S. Bae et al. [28] have developed a process (Figure 2.5) to build 30 inch graphene film on copper by using roll to roll method in 2010. After that, SONY has synthesized 100 meter long graphene film using the similar method in 2013 [29]. But the graphene coverage is not uniform and decreases when near the film edge. Also, there are defects caused by plastically deformation of copper foil. These non-negligible defects break the periodic structure and lower the conductivity of graphene [29]. Although in 2015 a new method called Concentric Tube CVD developed by Polsen, E. S. et al. [30] has improved the production speed and quality, the cost of CVD methods are still too high considering the low yield.

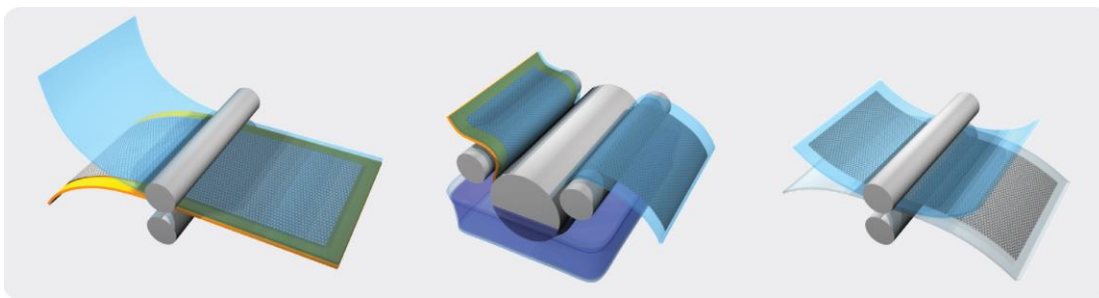


Figure 2.5 Schematic of the roll to roll method. The production process includes: adhesion of polymer supports, copper etching and dry transfer-printing on a target substrate. The figure was adapted from ref [28].

## 2.2 GRAPHENE OXIDE

Graphene oxide (GO) has a similar structure to graphene. Both of these compounds have a hexagonal carbon lattice, but the GO sheet is usually distorted where it is bonded to the oxygen groups. GO as one of the source materials for large-scale production of graphene has been studied for years. There are many applications for GO such as potential materials for electrode in Li-ion batteries [17], transparent conductor in organic photovoltaic cells [31]. Despite these advanced application, the fundamental determination of the structure of GO has been slow. Researchers have proposed many theoretical models for GO but the precise chemical structure is still controversial. Major reasons include sample-to-sample variability due to different synthesis methods the degree of oxidation, the amount of amorphization, the nonstoichiometric nature of GO, and the limited

resolution in the major characterization techniques such as SSNMR and FTIR. However, the determination of the precise structure of GO is still worthy of study because it will certainly improve the understanding of the functionalization and reduction process of GO.

## 2.2.1 Characterizations

### 2.2.1.1 Solid State $C^{13}$ Nuclear Magnetic Resonance (SSNMR) Spectroscopy

In 2008, Ruoff's group prepared a  $C^{13}$ -enriched GO sample and three broad resonances at 60, 70 and 130 ppm were discovered in the  $^{13}C$  SSNMR spectrum [32]. After that, SSNMR proved to be one of the most precise and reliable techniques to characterize GO structure. Figure 2.6 is reprinted from reference [32] which shows the 1D and 2D chemical-shift spectrum of  $C^{13}$ -labelled GO sample. The peaks clearly demonstrate the presence of  $sp^2$  carbon, epoxy and hydroxyl bonded carbon atoms. In later reports, the 101 ppm peak was identified and this peak represents the five or six-membered ring lactol structure[32].

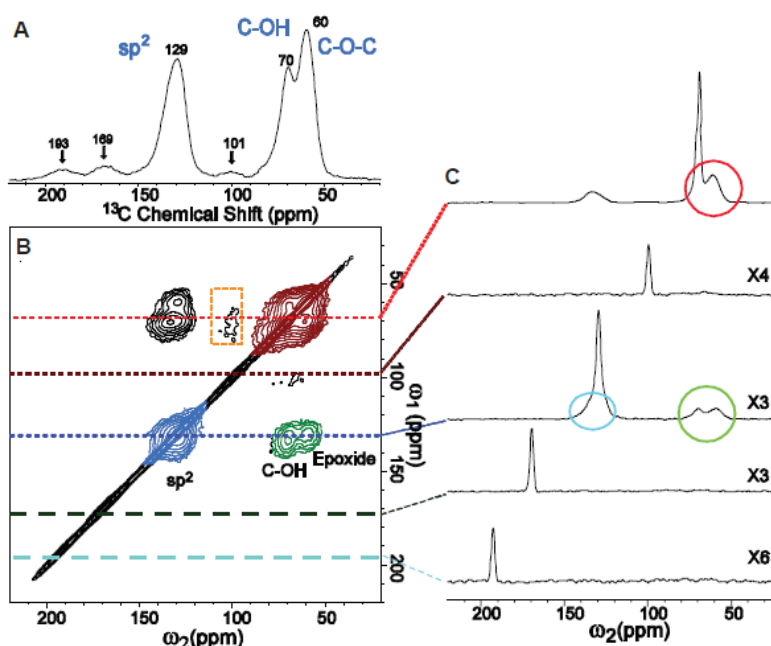


Figure 2.6 (A) 1D  $C^{13}$  MAS and (B) 2D  $C^{13}/C^{13}$  chemical-shift correlation solid-state NMR spectra of  $C^{13}$ -labeled graphite oxide with (C) slices selected from the 2D spectrum at the indicated positions (70, 101, 130, 169, and 193 ppm) in the  $w_1$  dimension. This figure was adapted from ref [32].

### 2.2.1.2 Other common methods

#### FTIR (Fourier transform infrared spectroscopy)

Besides SSNMR, FTIR is also a powerful tool to detect the functionalities on GO. But the large quantities of water molecules in GO structure make the hydroxyl groups undistinguishable. In 2005, Décány's group developed the DRIFT analysis [33] and clarified major peaks of a GO sample made

by Brodie method [34]. They distinguished the hydroxyl signals from water and thus end the previous debate on GO FTIR results. The FTIR spectrum (Figure 1.7 a ) gives the possible functionalities: carboxyl, lactone, phenol, lactol, chromene, ketone, etheric rings, organic carbonate, but definitely no pyrones [33].

### UV-vis (Ultraviolet-visible spectroscopy)

UV-vis spectrum (Figure 1.7 b ) shows two assigned bands at 234 nm and 299 nm, resulting from the  $\pi$  to  $\pi^*$  transition of aromatic carbon bonds C=C and n to  $\pi^*$  transition of C=O bonds [35].

### Raman spectroscopy

Raman spectroscopy is a non-destructive method that can detect the structural defects of GO. There are two major peaks (Figure 1.7 c), D peak at  $1350\text{ cm}^{-1}$  and G peak at  $1594\text{ cm}^{-1}$  corresponding to structural defects and graphene-like vibration respectively. However, the D/G ratio usually increases rather than decreases after the chemical reduction GO. There is an examination that this phenomenon is caused by the size diminishment of the re-established G network [36].

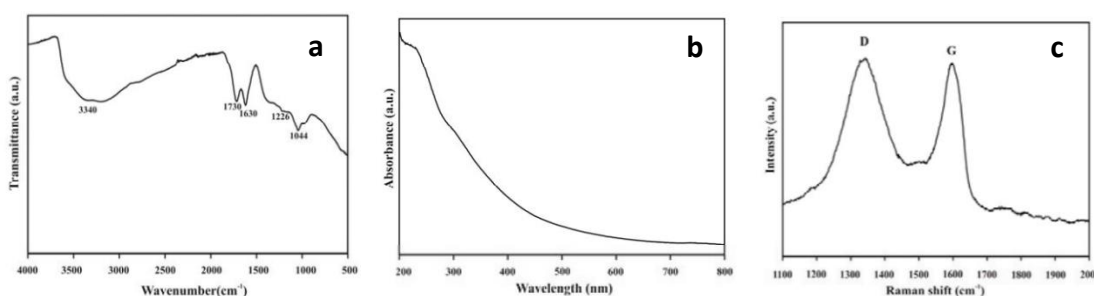


Figure 2.7 (a) FTIR spectrum of GO; (b) UV-vis spectrum (c) Raman spectrum [1]

### XRD (X-ray diffraction spectroscopy)

In the X-ray diffraction spectroscopy (Figure 2.8a ) , GO usually exhibits a broad peak at 10.2 degrees distinguished from graphene at 16.7 degrees [37].

### XPS (X-ray photoelectron spectroscopy)

X-ray photoelectron spectroscopy (Figure 2.8b ) shows binding energy peaks at 284.4 eV (C=C bonds), 286.8 eV (C-O bonds) and 288.7 eV (C=O bonds) [38].

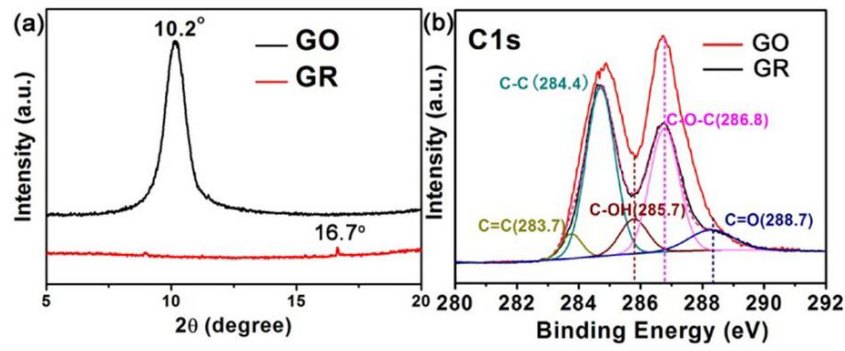


Figure 2.8 (a) XRD spectrum of graphene oxide (GO) and graphene (GR); (b) XPS spectrum of GO and GR. [37]

## TEM and AFM

Transmission Electron Microscopy (TEM) and Atomic Force Microscopy (AFM) reveals the two dimensional structure of GO (Figure 1.9). TEM could easily confirm the hexagonal graphene-like lattice of GO while the AFM observed a roughness of at least 0.6 nm on GO surface [2].

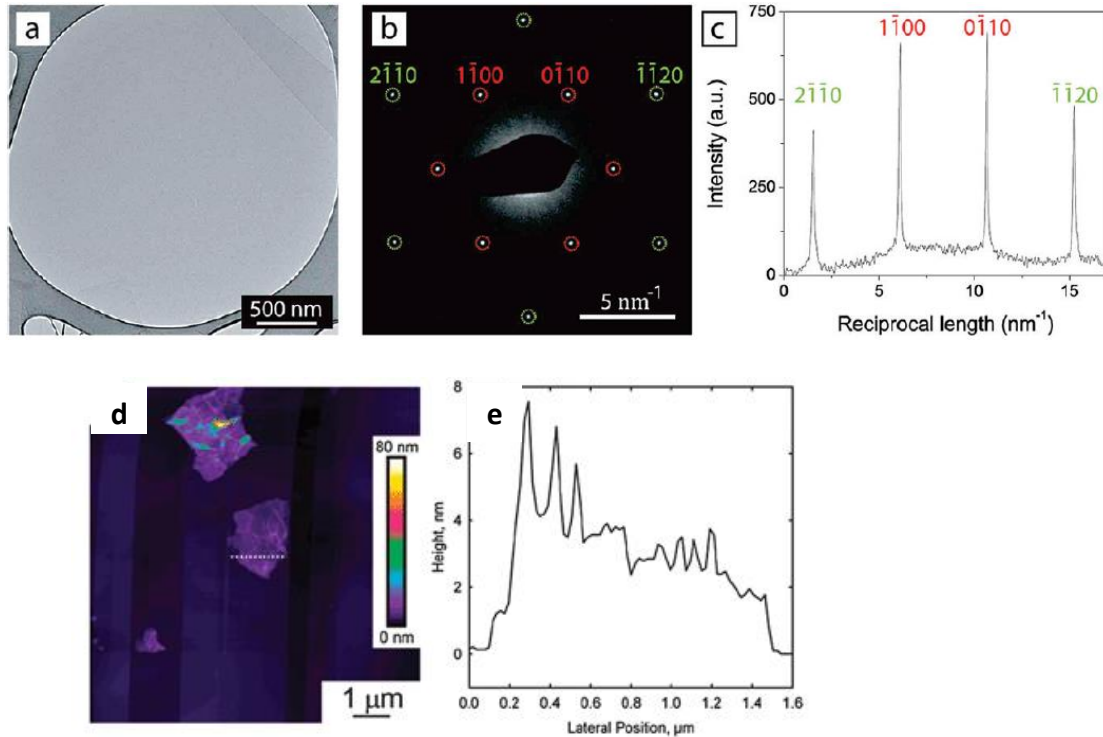


Figure 2.9 (a) TEM image of a single GO sheet on a carbon support. (b) Labelled SAED of the GO sheet in a. (c) Intensity profile through the diffraction spots labelled in panel b. (d) Contact-mode AFM scan of reduced graphene oxide etched on a graphene oxide paper substrate (e) Height profile through the dashed line shown in (d) The figure was adapted from ref [2]

## TGA

Thermal gravimetric analysis tests the thermal stability of GO. In most cases, GO decomposes from around 70 °C and is very unstable during the heating process [39].

## 2.2.2 Chemical structure

According to the characterization above, previous researchers have proposed at least 6 classic structure models (Figure 2.10) [25, 33, 40-43].

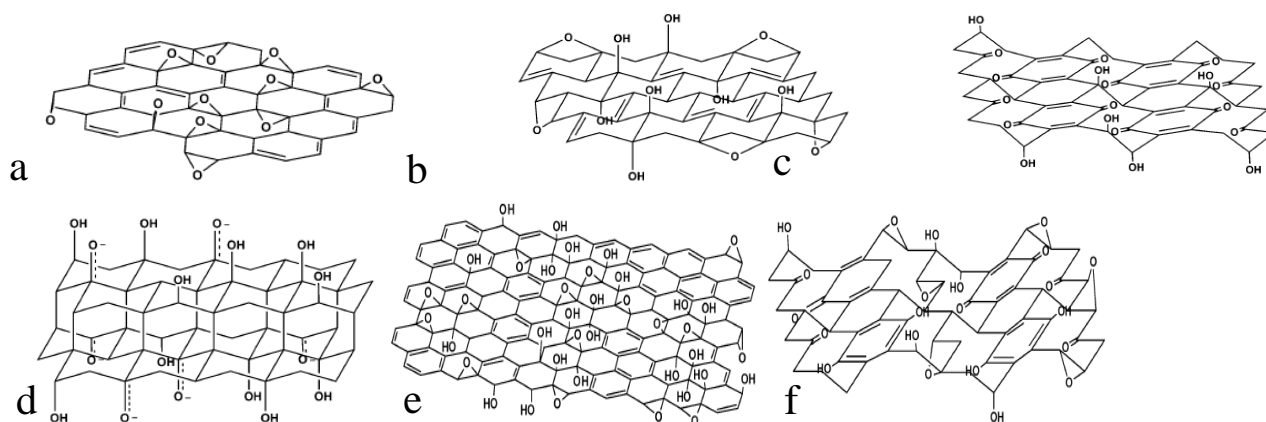


Figure 2.10 (a) Hofmann model; (b) Ruess model ; (c) Scholz-Boehm model ; (d) Nakajima-Matsuo model ; (e) Lerf-Klinowski model; (f) Dekany model [42]

The first model by Hofmann and Holst in 1939 describes a flat carbon sheet randomly bonded with epoxy groups with a C/O ratio of 2. Then in 1946, Ruess's group introduced the hydroxyl groups and 1, 3-ether to the lattice [44]. The lattice is composed by cyclohexane rings which are different from Hofmann's benzene-like carbon plane. Scholz-Boehm model [43] completely replaces the epoxide groups with hydroxyl groups. The basal plane is regular corrugated cyclohexane rings linked with a quinoidal structure. Nakajima and Matsuo 1994, built a lattice framework akin to poly (C<sub>2</sub>F)<sub>n</sub> which forms a stage 2 graphite intercalation compound[45]. However, the latest two models proposed by Lerf-Klinowski [40] and D é ány [33] have become most popular because the SSNMR analysis was introduced into GO structure characterization. This new technique has improved the accuracy in detecting the functional groups on GO. In the Lerf-Klinowski (LK) model, tertiary alcohols and 1, 2-ethers are dominant groups on the GO surface[40]. The LK model discards the periodic crystal structure and substituted by the randomly distributed oxygen groups. They also suggested that the alkenes (C=C) in GO are probably either aromatic or conjugated and ketones are more preferable at the edge of GO. Later, D é ány proposed a model following the basic logic of Scholz-Boehm model, but adding 1, 3-ethers into the cyclohexane rings [42].

As mentioned before, Rouff's group used the <sup>13</sup>C-labelled SSNMR to analyse the GO structure and compared the experiment data with the ab initio chemical shift calculations. Their conclusion indicates that only the LK model fits best with the experiment results while all other models were excluded due to their inconformity [44]. But due to the computation complexity, the size of the LK model used in calculation was simplified and limited in size. Therefore, the precise distribution of functional groups and the edge structure are still controversial.

Apart from the experimental results, the theoretical characterization of the GO structure can give us a new perspective into the detail structure of GO. Lahaye et al. calculated the hydroxyl and epoxy system in 2×2 GO cell using density functional theory (DFT) [46] where they found that the 1,3-ether are not likely to exist because of the joint binding energy and the single epoxy and hydroxyl prefer staying in close proximity. Boukhvalov and Katsnelson proposed a chainlike structure and found the band gap increased with the increasing oxygen coverage[47]. They also discovered that graphene has a high flexibility as the chemisorption results in 5 Å (radius) distortions of the graphene sheet for the presence of a single hydrogen atom [48]. As for the chemisorption of two hydrogen atoms, the most energetic favourable configuration is that two hydrogen are bonded to neighbouring carbons from the opposite sheet sides [4]. And the complete coverage of hydrogen atoms can minimize the total energy of graphene sheet [4]. This result was also theoretically confirmed by Yan and Chou [49] using MD (Molecular Dynamics) simulations and the transformation of hydroxyl and epoxy groups into carbonyl group during thermal annealing was revealed. The importance of hydrogen bonding was also proposed by Paci et al. in their Monte Carlo simulations [50]. Also, epoxide groups were observed to migrate on the basal plane in processes often stabilized by hydrogen bonding or catalyzed by hydrogen transfer reactions between the mobile epoxide oxygen and neighbouring functional groups[50]. Li et al. found that epoxy pairs aligning in line in graphene oxide plane are likely to form carbonyl pairs and then lead to the “unzip” of the GO sheet [51]. This result suggests a way to get a smooth GO edge by controlled oxidation process.

## 2.3 RESEARCH GAPS

In spite of such many theoretical models, the real structure of GO still remains controversial. One reason may be that these models arrange the oxygen groups manually in a fixed cell within a limited scale. But the real GO is non-stoichiometric and non-periodic in the long range. As a consequence, in this study, a new defect-free GO structure will be discussed both in a large scale molecular mechanics (MM) model and a precise density functional theory (DFT) model, so that both the long range pattern and the local interaction can be simulated and studied.

Both MM and DFT are complementary methods. The MM models are limited non-periodic models, but the MM method is fast and reliable which is good for massive screening computation to locate the most energetic favorable structure, while the DFT models are periodic models with unlimited scale, it provides a deeper insight for the chemical and electronic structures. The disadvantage of the DFT approach is the specific requirement of computational resource, and it will be extremely time-consuming to perform DFT calculations using a supercell containing hundreds of atoms. Based on these considerations, in this study, we use MM2 to search for structure and use DFT to

understand the structure. The scale limit is still there, but we can acquire more information from this combined method. Depending on the synthesis process, highly oxidized GO has different compositions varying from  $C_{1.5}O$  to  $C_{2.5}O$  [13, 14]. The fully oxidized area of GO model in this study has a C/O ratio of 1.5:1 which is close to the composition of commercial GO such as products from ACS Material®.

## Chapter 3. COMPUTATIONAL METHODS

The thermodynamic GO model proposed in this study refines the LK model [40]. In our proposed model, the epoxide groups and hydroxyl groups distribute randomly over a long range while having a local energy-favorable pattern. The new thermodynamic model depicts the interactions between the functional groups in both MM and DFT methods, leading to a more accurate description of the local GO structure.

In this study, the hexagonal GO supercells with a size varying from 6 to 54 carbon atoms are built to estimate the steric energy ( $E_{steric}$ ) [9]. The equilibrium covalent geometry of molecules can be precisely reproduced by MM2 force field, and  $E_{steric}$  can be calculated using the following equation [9]:

$$E_{steric} = \sum_{bonds} K_r (r - r_{eq})^2 + \sum_{angles} K_\theta (\theta - \theta_{eq})^2 + \sum_{dihedrals} \frac{V_n}{2} [1 + \cos(n\varphi - \gamma)] + \sum_{non-bonded} \left[ \frac{A_{ij}}{R_{ij}^{12}} - \frac{B_{ij}}{R_{ij}^6} + \frac{q_i q_j}{\epsilon R_{ij}} \right] + \sum_{H-bonded} \left[ \frac{C_{ij}}{R_{ij}^{12}} - \frac{D_{ij}}{R_{ij}^{10}} \right], \quad (1)$$

where the equilibrium length  $r$  and angle  $\theta$  are determined by atom/bonds types and location.  $K$  is a force constant controlling the bond stretching (first term) and bending stiffness (second term). The third dihedral term using Fourier series represents the torsional interaction considering the single and double bonds, where  $V$  is the torsional rotation force constant and  $\varphi$  is the torsional angle. The fourth term describes the non-bonded interactions, where  $\epsilon$  is the permittivity of free space,  $q_{i/j}$  are atomic charges, and  $R_{ij}$  is the distance between atom  $i$  and  $j$ , respectively. The fifth term describes  $\pi$ -conjugation, hydrogen bonding or anomeric effects, where the  $A$ ,  $B$ ,  $C$ ,  $D$  are all suitable constants [9]. The initial GO models were graphene-like sheets and built with C-O bond length of 1.42 Å and C-C bond length of 1.42 Å which are the values in CO and pure graphene. From which, the initial GO structure can be relaxed by MM2 force field, and  $E_{steric}$  was used to comparing the structural stability of different models with same chemical stoichiometry.

To clarify the interaction between functional groups and in turn the influence on electronic structure, the DFT calculations were performed using both Gaussian [52] and WIEN2k program suites. Gaussian 09 [52] is an electronic structure modelling software using ab initio, density functional theory, semi-empirical, molecular mechanics, and various hybrid methods. It can perform geometry optimisation using internal co-ordinates. The basic approach of the calculation is for the charge carriers in the supercell to be moved around stepwise until the step energy or the forces applied on the atoms fall below a specified tolerance value. The Berny algorithm using GEDIIS [53] in redundant internal coordinates [54-59] is used in optimization of atomic positions.



Constructs of  $4 \times 4$  graphene-like supercells containing 16 carbon atoms were used as a basis for the GO models. The initial lattice parameters of  $a=4.92 \text{ \AA}$ ,  $b=8.52 \text{ \AA}$ ,  $c=10.00 \text{ \AA}$  were derived from the normal  $1.42 \text{ \AA}$  C-C bond. The  $10.00 \text{ \AA}$  vacuum-separation along the c-axis was built to minimize the coulombic interaction between layers. A number of algorithms were used in the 6-31g (d) basis set for modelling carbon and oxygen atoms and Perdew–Burke–Ernzerhof (PBE) [60] functional in the geometry optimization process. In each self-consistent field cycle, the total energy generated by the Kohn-Sham equations [61] is compared with previous configurations and checked if forces are within tolerance limits. The self-consistent field cycle ends until the forces fall below a predefined tolerance and reach the minimum energy.

WIEN2k is an all-electron computational code including relativistic effects [62, 63]. The electronic structure of GO models can be calculated by full-potential (linearized) augmented plane-wave ((L) APW) + local orbitals (LO) method, which is known as one of the most precise method for calculating band structures[62]. During the calculation, generalized gradient approximation of Perdew-Burke-Ernzerhof 96 (GGA-PBE) and Monkhorst–Pack (mesh) approximation [64] were used to collect exchange–correlation potential [62, 65]. To investigate the influence of hydroxyl-chain and epoxy-chain on the GO band structure, a  $2 \times 2$  supercell containing 4 carbon atoms and 1 oxygen atom was built. The number of k-points was 1000 and the separation energy was set as  $-6.0 \text{ Rydbergs}$  [66].

## Chapter 4. RESULTS AND DISCUSSION

### 4.1 DETERMINATION OF THERMODYNAMICALLY STABLE STRUCTURES

MM calculations were used to search and determine the most thermodynamically stable structures of GO. The elementary unit of GO in the MM models is defined as a single benzene ring containing 6 carbon atoms and 4 oxygen atoms. Hydroxyl and 1, 2-ethers are two basic functional groups on the both sides of the GO sheet, so that their relative positions were firstly studied. Figure 4.1 displays the cis-configuration and trans-configuration  $C_{72}O(OH)$  models and  $E_{steric}$  calculated by MM method. The results are consistent with previous theoretical studies [46, 49, 67-69] that the nearby hydroxyl and epoxy groups tend to locate on the opposite sides of the GO sheet. This tendency can be explained by the structure distortion and tension using the MM theory.

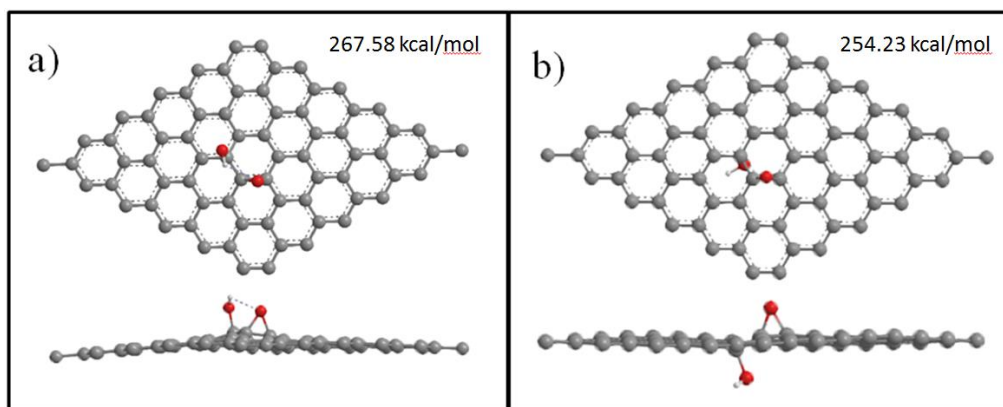


Figure 4.1 MM models view from top and side: a)  $C_{72}O(OH)$  in cis-configuration and b)  $C_{72}O(OH)$  in trans-configuration.

$E_{steric}$  can be calculated using Eq. (1) and their calculated values are listed in Figure 4.1. As can be seen, the trans-configuration has a lower inner stress which leads to a lower  $E_{steric}$  and the results are the same for models with two single epoxy groups or two single hydroxyl groups. According to the steric symmetry, there are 27 isomers of  $C_6O_4$  (detailed 27 schematic isomer models are presented in Appendix 1). The constraining conditions of building GO isomer models are the fixed C:O ratio of 1.5 and the coexistence of hydroxyl and epoxide groups. Therefore, these isomers can be classified into 4 major types that can be distinguished by the different substitution sites of functional groups. Figure 4.2 shows the 4 most stable structure of each type: type A: 1, 3-epoxy substituted  $C_6O_2(OH)_2$ ; type B: 1, 4-epoxy substituted  $C_6O_2(OH)_2$ ; type C: 1, 2, 3-hydroxyl substituted  $C_6O_1(OH)_3$ , and type D: 1, 2, 4-hydroxyl substituted  $C_6O_1(OH)_3$ . Each isomer was embodied in a  $C_{54}$ -hexagonal graphene sheet and fully relaxed.  $E_{steric}$  for individual isomers were

calculated and listed in Figure 4.2. The comparison of  $E_{steric}$  for individual isomers indicates that the type B model with two para-substituted epoxides and two para-substituted hydroxyls is the most energetically favorable structure with  $E_{steric} = 20.89 \text{ kcal/mol}$ .

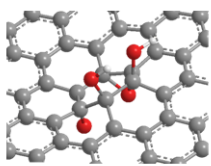
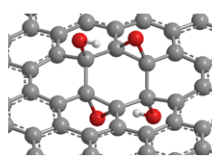
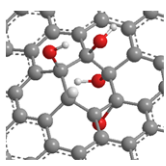
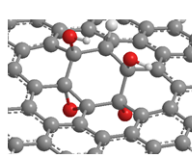
A	B	C	D
			
27.45 kcal/mol	20.89 kcal/mol	47.65 kcal/mol	21.67 kcal/mol

Figure 4.2  $C_6O_4$  models and MM steric energies.

To determine the stable structure type with the high O/C ratios, we increase the oxygen atoms to 16 and 36 on the  $C_{54}$  graphene frame. Consequently, both  $C_{54}O_{16}$  and  $C_{54}O_{36}$  supercells were derived from the basic  $C_6O_4$  cell and also can be classified into the same 4 types. The  $C_{54}O_{16}$  and  $C_{54}O_{36}$  models with their calculated  $E_{steric}$  values are listed in Figure 4.3, which shows the distribution of the functional groups in larger models still follows the most stable configuration discovered in the  $C_6O_4$  models shown in Figure 4.2.

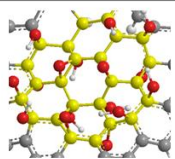
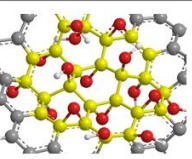
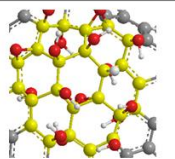
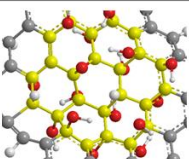
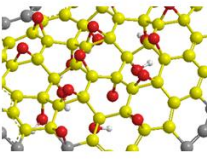
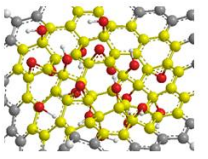
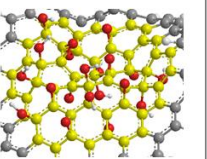
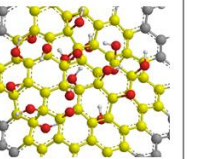
	A	B	C	D
$C_{24}O_{16}$				
	2245.13 kcal/mol	1854.61 kcal/mol	2222.89 kcal/mol	2003.09 kcal/mol
$C_{54}O_{36}$				
	3747.00 kcal/mol	3465.28 kcal/mol	3794.71 kcal/mol	3913.07 kcal/mol

Figure 4.3  $C_{24}O_{16}$  and  $C_{54}O_{36}$  models steric energies.

The comparison of different  $E_{steric}$  values calculated based on different  $C_{24}O_{16}$  models verified the type B (1, 4-trans-epoxy) as the most stable case. With increasing the number of atoms in the super cell, there are some equivalent positions for the hydroxyl groups. These varieties were ignored during the calculation because the hydroxyls on equivalent positions contribute the same to the total energy. In the most stable type B model, the hydroxyl bond (red atom in Figure 4.4, H atom hidden) still remains approximately perpendicular to the plane formed by the three  $\beta$ -C atoms. This stable orientation results from the equal tension caused by  $sp^3$  hybridization between  $\alpha$ -C and  $\beta$ -C [70]

(refer to Figure 4.4). Based on the MM2 dynamics calculation, the free-standing hydroxyls are not likely to interact with the neighboring carbon atoms.

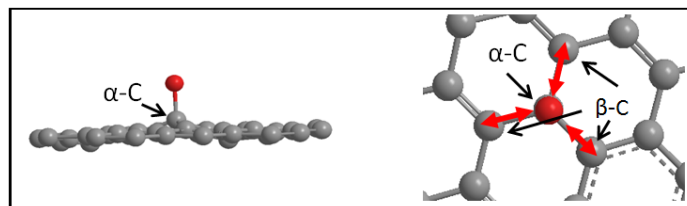


Figure 4.4 Tension caused by  $sp^3$  hybridization between  $\alpha$ -C and  $\beta$ -C (red arrows); two carbon positions:  $\alpha$ -C, directly bonded to oxygen;  $\beta$ -C, three atoms bonded to  $\alpha$ -C.

The comparison of  $E_{steric}$  values obtained from different  $C_{54}O_{36}$  models also confirm the previous inference that the type B structure (1, 4-trans-epoxy) with two para-substituted epoxides and two para-substituted hydroxyls is the most energetic favorable structure. However, the  $C_{54}O_{36}$  supercell illustrates a more complicated local environment for the epoxides and hydroxyls. The distribution of trans-configuration of the epoxides and hydroxyls is limited because the increased system complexity induces metastable states. These metastable states allow the co-occurrence of the neighboring epoxide and hydroxyl on the same side of GO sheet. Kim *et al.*[71] also discovered the metastable characteristics of graphene oxide produced by the Hummers method and the structural relaxation time at room temperature was about one month. The simulation of metastable GO structural relaxation suggested the diffusion of neighboring oxygen atoms [71].

We now consider the GO edge structure which were often ignored in theoretical calculation [72]. The edge structure is modelled in a  $4 \times 4$  graphene flake with only one side decorated by carbonyl, carboxyl and hydroxyl groups. The calculated  $E_{steric}$  are listed in Table 1 that shows the preferred orientation of the edge functional groups. Each functional group is bonded to GO models in two characteristic orientations and calculated  $E_{steric}$  values for different GO edge models are listed in Table 1 as well.

Table 1 GO edge model and MM steric energies

Functional group	Carbonyl		Carboxyl		Hydrxyl	
Orientation	Zigzag	Armchair	Zigzag	Armchair	Zigzag	Armchair
GO Edge Models						
Steric Energy (kcal/mol)	26.5281	52.8723	26.4628	0.6027	26.4628	26.8975

The comparison of obtained  $E_{steric}$  values, it can be found that the armchair-carboxyl has the lowest  $E_{steric}$ , while the armchair-carbonyl has the highest  $E_{steric}$ . For this reason, at the edge of the GO sheet, the carboxyl prefers attachment along the armchair orientation, while the carbonyls prefer attachment in the zigzag orientation.

## 4.2 INTERACTION OF FUNCTIONAL GROUPS

Since the type B (1, 4-trans-epoxy) structure is the most energetically favorable structure, our DFT calculations are only performed based on this structure to study the interaction of the bonded functional groups. In the new  $2 \times 2$  periodic supercell, the type B structure consists of 4 para-substituted epoxides and 8 para-substituted hydroxyls in trans-configuration as shown in Figure 4.5a.

For comparison, we also consider a promising model containing only hydroxyls and epoxide functional groups in a hydroxyl-chain configuration as shown in Figure 4.5b [47, 49]. In this model, a long chainlike structure formed by 1, 2-hydroxyl pairs on both sides of the GO sheet. The hydrogen bonds between the hydroxyls play an important role to stabilize the structure. However, as a consequence, the concentration of hydroxyl groups stays at a high level that is not consistent with recent nuclear magnetic resonance signatures of GO [69, 73, 74]. The experimental nuclear magnetic resonance spectrum does not show a broadened hydroxyl peak [69, 74], so that the chainlike structure might exist but not be a dominant configuration.

The type B model in this study also has a controversial structure, that is, the para-substituted epoxide functional groups. Li *et al.* [75] found that if the epoxy groups are aligned, they are likely to break apart the graphene sheet by splitting into carbonyl pairs. This mechanism is also believed to be one of the main causes for linear defects in GO [67, 75]. For this reason, to clarify the stability of epoxy chainlike structure, the DFT calculations were performed to compare the two models both energetically and electronically.

The binding energy ( $E_b$ ) of GO was calculated using a function of oxygen and hydrogen chemical potentials ( $\mu$ ) [76]:

$$E_b = E_{tot}(C_l O_m H_n) - E_{tot}(C_l) - m\mu_O - n\mu_H, \quad (2)$$

where  $E_{tot}(C_l O_m H_n)$  and  $E_{tot}(C_l)$  are the total energy of GO and pristine graphene supercells with  $l$  C atoms,  $m$  O atoms and  $n$  H atoms. Using Eq. (2),  $E_b = -3.28$  eV can be obtained from the configuration shown in Figure 4.5a, which is 1.31 eV lower than  $E_b = -1.97$  eV for the configuration shown in Figure 4.5b. In Figure 4.5a, the epoxy group enlarges the C-C bond from the original 1.42 Å to 1.44 Å, and the C-C bonds near the hydroxyls vary from 1.48 Å to 1.52 Å which is very close to C-C bond length of 1.50 Å [77] for mixed  $sp^3-sp^2$  hybridized bonding. In

Figure 4.5b, the C-C bond under epoxy group is similar to Figure 4.5a, but the C-C bond between two hydroxyls is 1.54 Å which is the length of the C-C bond in the diamond structure [70]. Based on this, these two models are both in agreement with previously predicted lattice distortions in GO.

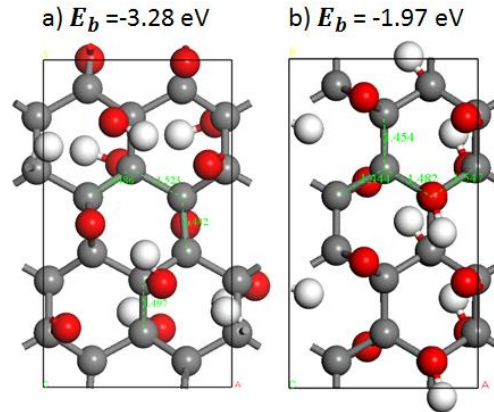


Figure 4.5 Supercells of: a) 1, 4-trans-epoxy structure; b) chainlike structure. The grey, red and white spheres represent carbon, oxygen and hydrogen atoms respectively. The determined  $E_b$  is shown at the top.

It is of interest to note the chainlike hydrogen bonding in Figure 4.5b does not show the energetic advantage in our calculations. The reasons can be explained in Figure 4.6, in which the electron density map displays the complicated H-bond network in the 1, 4-trans-epoxy model. There exist two types of H-bonds: (1) H-bond forms between two hydroxyl groups and the second type of H-bond can be found between hydroxyl and epoxy groups. In addition, the second type H-bonds show a higher electron density in some locations than its first type counterpart. The average length of the first type H-bond (H---O) is 1.75 Å, which is shorter than the average length of 1.90 Å for the second type H-bond. Also, both are shorter than the H-bond length of 1.97 Å between water molecules [78]. According to the Jeffrey's definition [78], the H-bond between 1.5 Å to 2.0 Å is considered as the moderate H-bond with the bonding energy of 0.17eV to 0.65eV. The interaction of the H-bonds thus plays an important role in building the GO structure. Since the H-bond networks are complicated, the H-bonds in the chainlike structure are not likely to make a significant difference to the total energy. However, for the type B structure shown in Figure 4.6a, the H-bond networks can decrease  $E_b$  and stabilize the structure.

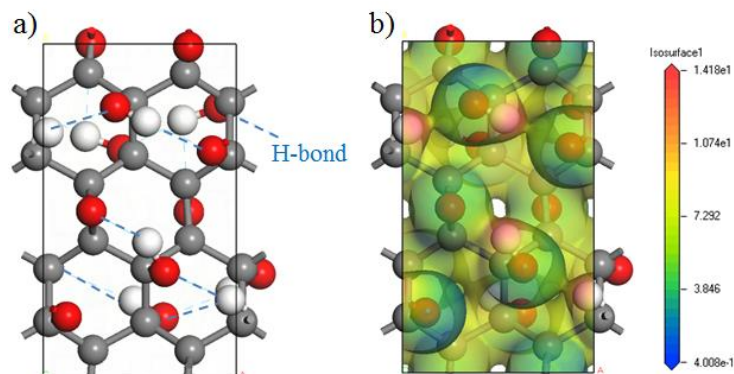


Figure 4.6 a) H-bonds (blue dashed lines) sketch in GO; b) Charge density map of the b-type GO model.



Li *et al.*[51] found that the epoxy pairs that align with single side of GO sheet are likely to form carbonyl pairs, causing the GO sheet to disassemble [51], However, in our proposed type B model, the epoxy chain does not lead to the sheet separation. For this reason, the trans- and cis-configuration of GO models containing only the aligned epoxy groups were calculated. Figure 4.6 shows the results and indicates that the para-substituted epoxide functional groups are likely to cause GO sheet to disassemble. In the case of cis-configuration (Figure 4.6a and Figure 4.6b), all the epoxide functional groups locate on the same sides of the graphene sheet, the GO sheet is separated by a linear chain of epoxide functional groups and a wrinkle appears with an angle of  $101.5^\circ$ . The distance between the two carbon atoms under the epoxy group is  $2.15 \text{ \AA}$ , which is much larger than a normal C-C bond of  $1.54 \text{ \AA}$ . In the case of trans-configuration (refer to Figure 4.7c and d), the epoxide functional groups exist on both sides of the graphene sheet; the GO sheet is just slightly distorted rather than disassembled. We also calculated  $E_b$  for different epoxy pair structure and their values are listed in Figure 4.7b and 7d. As can be seen,  $E_b = -4.31 \text{ eV}$  in the Figure 4.7d model is  $1.12 \text{ eV}$  higher than  $E_b = -5.43 \text{ eV}$  of the fractured Figure 4.7b model, so that the cis-configuration of epoxy pairs is more energetically favorable. This result indicates that there is a high chance for GO lattice with epoxy chains to form defects or break into small flakes during the synthesis process [79-81]. As a consequence, the trans-configuration of epoxide groups remains in unbroken and defect-free GO structure.

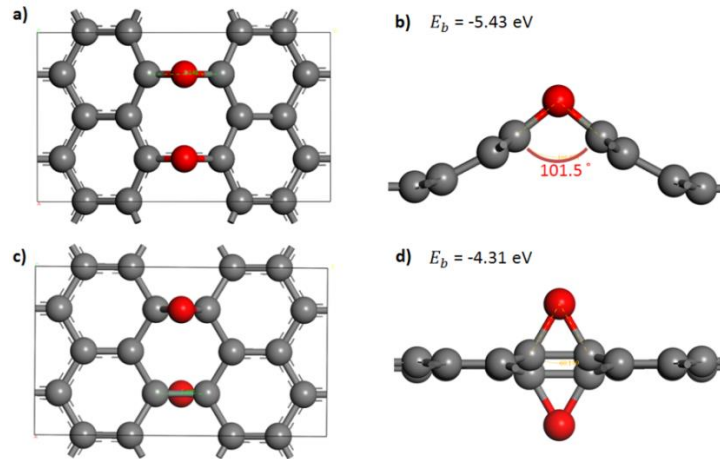


Figure 4.7 Supercells of a), b) Cis-configuration GO model with two epoxy groups; c), d) Trans-configuration GO model with two epoxy groups. The total energy is shown above the side-view model.

### 4.3 ELECTRONIC PROPERTIES

GO is regarded as a promising transparent conductor in photovoltaic cells [17, 31]. For their potential applications, it is important to understand the electronic properties of different GO models caused by the changing oxygen functional groups. For this reason, we calculate the band structure of the  $1 \times 1$  graphene and GO models using the WIEN2k program suite. Figure 4.8a presents the

band structure of pristine graphene (for comparison) which shows the typical Dirac point in the  $k$  space, and Figure 4.8b displays the band structure of GO with hydroxyl groups only. In our case of hydroxyl, the existence of the hydroxyl groups breaks the symmetry of graphene and opens a small band gap of 0.22 eV. Figure 4.8c shows the band structure of GO with epoxide groups, in which a larger band gap of 1.0 eV is seen. Different from the strong delocalization band in graphene, both the hydroxyl groups and epoxide groups induce the flat localized band near the Fermi level in GO. The electron transportation is believed to be hindered by the induced localized states [82]. This band structure results from the strong covalent C-O bonding which change the carbon bond from  $sp^2$  to  $sp^3$ . A similar calculated band gap of 0.9 eV of GO with epoxide was reported by Mattson *et al.*[83] and a 1 eV band gap was observed experimentally in the reduced GO [84]. It was also reported that GO acceptors with band gap ranging from 1 to 3 eV is highly desirable to accomplish high power conversion efficiencies in polymer solar cells [85]. To estimate the effect of functional groups on energy gap, the density of states corresponding to models shown in Figure 4.5a and b were calculated and the results are shown in Figure 4.9.

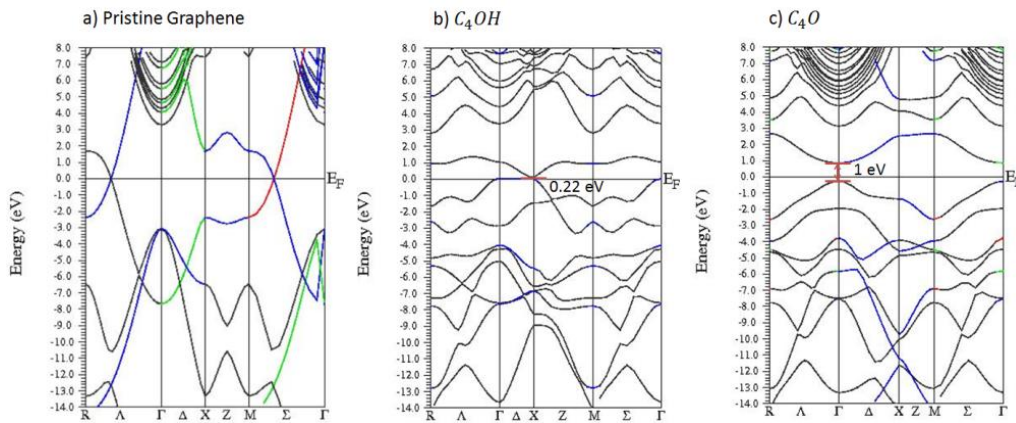


Figure 4.8 Band structures of pristine graphene a) and GO with b) a single hydroxyl, and c) a single epoxy. All using a  $2 \times 2$  supercell.

The density of states of the 1, 4-trans-epoxy GO model shown in Figure 4.9a can be identified by the 2s orbital peaks at  $\sim -23$  eV, and  $-21$  eV, corresponding to the epoxide group and hydroxyl group, respectively. In Figure 4.9b, hydroxyl chain structure leads to two strong peaks at  $-21$  eV and  $-22$  eV. Both models show strong peaks near the Fermi level, leading to a strong electron localization. In contrast, a relatively flat peak was observed at the position of epoxide 2s orbital in Figure 4.9c and the delocalization states of pristine graphene were partially restored. The energy gap of the full oxidized GO model increases from 3 eV to 4 eV when the hydroxyl chain structure is replaced by 1, 4-trans-epoxy structure. This result is consistent with Figure 4.8, in which the periodic hydroxyl chain can narrow the energy gap when compared to the epoxy chain structure. Also, as the oxidation of GO is a highly non-equilibrium process, the pristine graphene area with



$sp^2$  carbon bond was often observed in experiments [32, 35, 36, 38]. These un-oxidized graphene areas lead to a significant decrease of the GO band gap to 2 eV as shown in Figure 4.9c. As a consequence, the band gap of GO can be theoretically tuned by two approaches: (1) chemical reduction of GO to increase the  $sp^2$ -carbon area, and (2) controlled oxidation process of GO to adjust the distribution of functional groups. Both methods have been reported effective in recent experiments [85, 86].

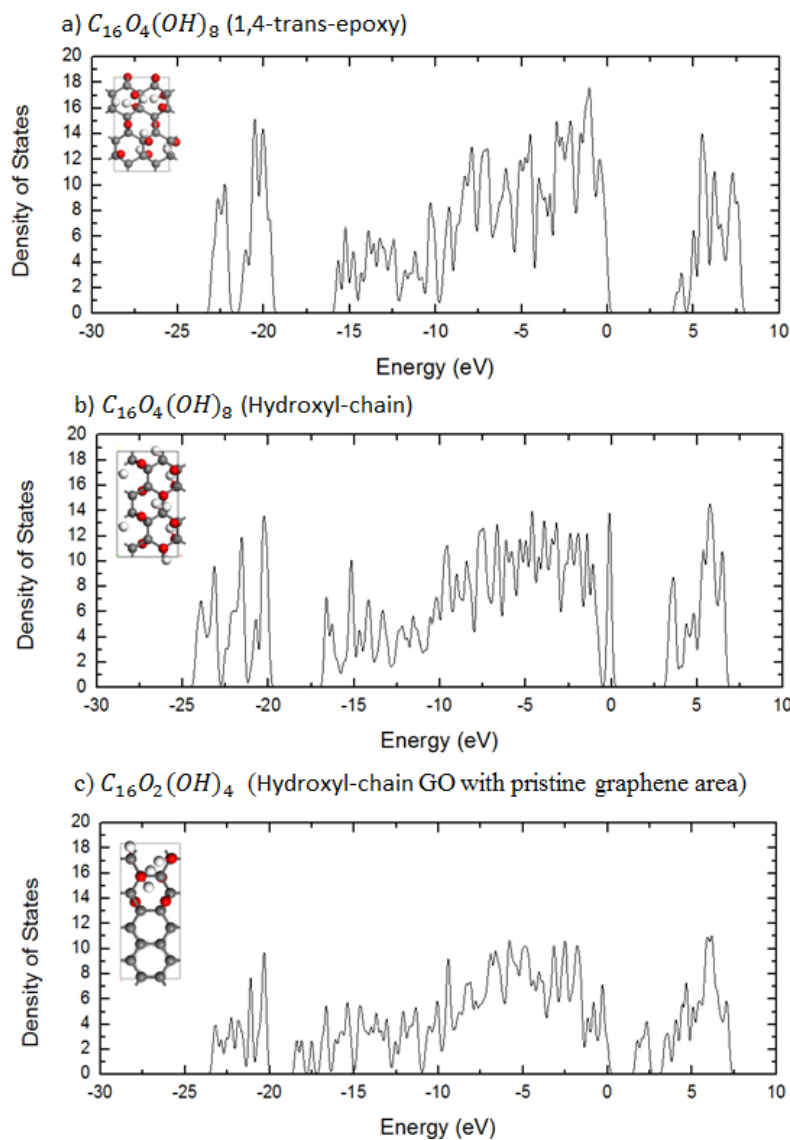


Figure 4.9 Density of states of a) hydroxyl chainlike structure; b) 1, 4-trans-epoxy structure c) 1, 4-trans-epoxy structure with pure graphene stripe area.

Based on our detailed analyses shown above, Figure 4.10 schematically illustrates our proposed thermodynamic GO structure containing two regions. (1) Graphene-like area with benzene rings and oxidized region with surface bounded oxygen groups. Two functional groups exist in each GO cell, that is, para-substituted epoxide groups with interspersed hydroxyl groups on two sides of the

GO sheet. (2) Pure graphene areas without any functional groups bonded. The ratio of these two regions depends mainly upon the GO oxidization level. At the edge of the GO sheet, the carboxyl prefers attachment along the armchair orientation, while the carbonyls prefer attachment in the zigzag orientation. The vacant edge carbon atoms are occupied by OH bonds.

The carbon grid has a moderate wrinkling due to the oxygen debris [87]. This deformation is located around hydroxyl and epoxide molecules where the  $sp^3$  hybridization is induced in C-C bonds. Despite the deformation, GO still maintains a hexagonal graphene-like structure. This structural stability results from the trans-configuration arrangement of the hydroxyl and epoxide oxygen, and the hydrogen networks also make an important contribution.

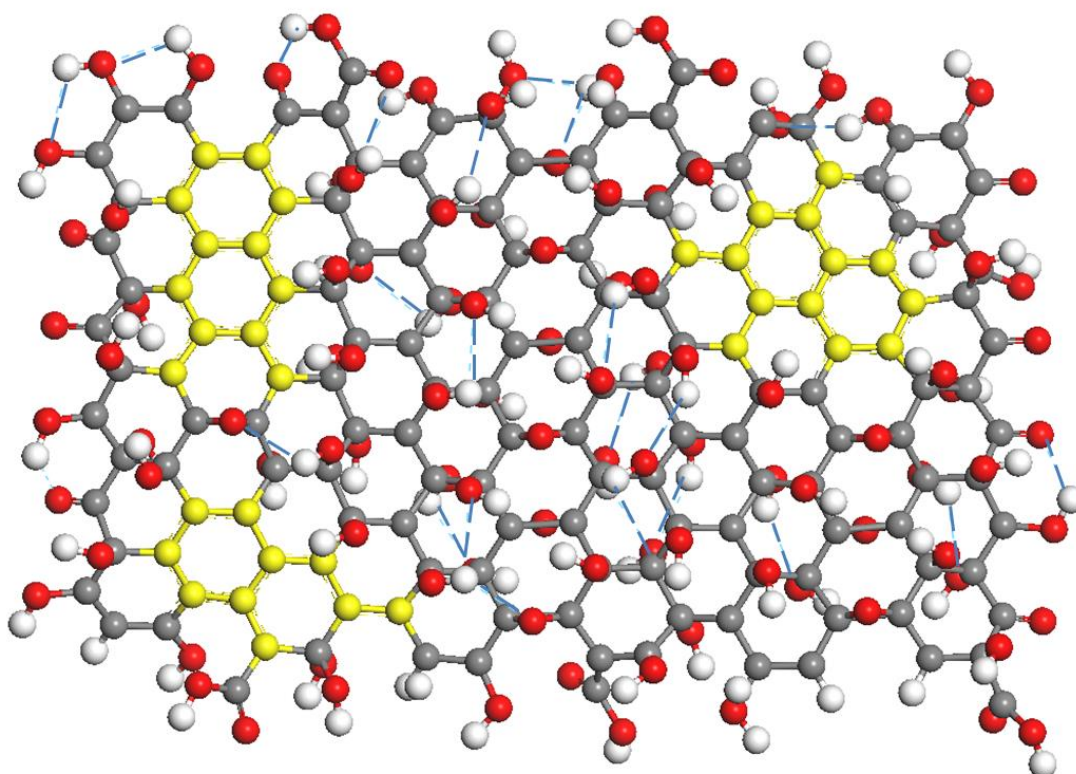


Figure 4.10 New Proposed thermodynamic GO structure model of GO. The grey, red and white spheres represent carbon, oxygen and hydrogen atoms respectively. The yellow areas represent pure graphene regions and the blue dashed lines represent the hydrogen bond networks.

## Chapter 5. CONCLUSION, LIMITATION AND FUTURE STUDIES

### 5.1 CONSLUSION

In this study, MM and DFT calculations were performed to determine the equilibrium structure of oxygen functional groups on GO and its electronic properties. A equilibrium GO structure is proposed that has the chemical formula  $C_{1.5}O:H$  which closely fits many experimental and

commercial products [14, 88]. The trans-configuration of hydroxyl and epoxide groups on GO is found to be energetically favorable and the local epoxide and hydroxyl chains also form the H-bond networks. GO with periodic epoxide chain structure has the semiconductor's electronic characteristic. It was also found that, by replacing epoxide with hydroxyl the band gap will decrease. The existence of pure graphene region also indicates that a well-controlled oxidation process can tune the band gap of the GO sheet. Furthermore, on the GO edge, the carboxyl prefers to attach the armchair orientation, while the carbonyl prefers the zigzag orientation.

## 5.2 LIMITATION

In this study, we did not simulate the reactions occurred during the oxidation process of GO but focused on the final stable structure. The structural model describes the preferable alignment of oxygen functional groups and also the related electronic properties. However, the limitation of this model is that it cannot provide information of the oxidation process which also plays an important role in forming stable GO structure. A further molecular dynamics simulation of GO can be conducted as a supplement of our model.

## 5.3 FUTURE WORK

With high conductivity and high transmittance, graphene is regarded as the potential transparent conductor to replace the conventional ITO (Indium Tin Oxide). However, under present techniques and equipment, the number of defects, the low yields, the limited size and the high cost prevent graphene from industrialized application. An alternative solution is depositing graphene or graphene oxide flakes onto the ITO surface to improve its electrical conductivity. Thus, a low cost, highly transparent and low resistance ITO-Graphene composite film can be expected.

ITO-Graphene or ITO-GO composites are a prominent transition material with relatively low cost and good performance between the traditional ITO and graphene. In 2011, Choi *et al.* [89] developed a solution process to synthesis reduced graphite oxide-ITO composites for use in transparent electrode. Adding the reduced graphite oxide has increased the conductivity of ITO electrodes. The sheet resistance of sol-gel ITO decreased from  $2 \times 10^3 \text{ } \Omega/\text{sq}$  to at least  $1 \times 10^3 \text{ } \Omega/\text{sq}$  while the optical transmittance remained as high as 87% [89]. And in 2013, H. Yang *et al.* [90] successfully prepared graphene nanosheet-ITO composites as an anode material for Li-ion batteries. This composite showed an improvement in reversible capacity, cycling stability, and rate capability of battery anode. The latest progress on ITO-graphene was made by Liu *et al.* [91]. They have synthesised a highly stretchable and flexible graphene-ITO hybrid transparent electrode with

transmittance of 88.9% and sheet resistance of 78.34  $\Omega/\text{sq}$ . Moreover, this material was developed using a two-step process to deposit the graphene on the ITO surface.

Although there is progress in ITO-Graphene or ITO-GO composites, the performance of the composites has not reached the ideal level for the real application. To explore the limit of the electrical and optical enhancement, theoretical modelling will be used to design new composites structure. And the major task of the modelling work is to achieve a balance between the electrical conductivity and optical transparency.

## REFERENCES

---

- [1] S. Chaikyakun, N. Witit-Anun, N. Nuntawong, P. Chindaudom, S. Oaew, C. Kedkeaw, *et al.*, "Preparation and characterization of graphene oxide nanosheets," *Procedia Engineering*, vol. 32, pp. 759-764, 2012.
- [2] N. R. Wilson, P. A. Pandey, R. Beanland, R. J. Young, I. A. Kinloch, L. Gong, *et al.*, "Graphene Oxide: Structural Analysis and Application as a Highly Transparent Support for Electron Microscopy," *Acs Nano*, vol. 3, pp. 2547-2556, Sep 2009.
- [3] K. S. Novoselov, A. K. Geim, S. V. Morozov, D. Jiang, Y. Zhang, S. V. Dubonos, *et al.*, "Electric field effect in atomically thin carbon films," *Science*, vol. 306, pp. 666-669, Oct 22 2004.
- [4] X. Huang, X. Qi, F. Boey, and H. Zhang, "Graphene-based composites," *Chemical Society Reviews*, vol. 41, pp. 666-686, 2012.
- [5] R. G. Gordon, "Criteria for choosing transparent conductors," *Mrs Bulletin*, vol. 25, pp. 52-57, Aug 2000.
- [6] M. J. Allen, V. C. Tung, and R. B. Kaner, "Honeycomb Carbon: A Review of Graphene," *Chemical Reviews*, vol. 110, pp. 132-145, Jan 2010.
- [7] W. Choi, I. Lahiri, R. Seelaboyina, and Y. S. Kang, "Synthesis of Graphene and Its Applications: A Review," *Critical Reviews in Solid State and Materials Sciences*, vol. 35, pp. 52-71, 2010.
- [8] Y. Zhang, L. Zhang, and C. Zhou, "Review of Chemical Vapor Deposition of Graphene and Related Applications," *Accounts of Chemical Research*, vol. 46, pp. 2329-2339, Oct 15 2013.
- [9] N. L. Allinger, "Conformational analysis. 130. MM2. A hydrocarbon force field utilizing V1 and V2 torsional terms," *Journal of the American Chemical Society*, vol. 99, pp. 8127-8134, 1977.
- [10] J. H. Son and T. R. Rybolt, "Force Field Based MM2 Molecule-Surface Binding Energies for Graphite and Graphene," *Graphene*, vol. 2, p. 18, 2013.
- [11] H. Elmsellem, M. Youssouf, A. Aouniti, T. B. Hadda, A. Chetouani, and B. Hammouti, "Adsorption and inhibition effect of curcumin on mild steel corrosion in hydrochloric acid," *Russian Journal of Applied Chemistry*, vol. 87, pp. 744-753, 2014.
- [12] N. L. Traulsen, C. H.-H. Traulsen, P. M. Deutinger, S. Müller, D. Schmidt, I. Linder, *et al.*, "Chelate cooperativity effects on the formation of di-and trivalent pseudo [2] rotaxanes with diketopiperazine threads and tetralactam wheels," *Organic & Biomolecular Chemistry*, vol. 13, pp. 10881-10887, 2015.
- [13] C. Valles, F. Beckert, L. Burk, R. Mulhaupt, R. J. Young, and I. A. Kinloch, "Effect of the C/O Ratio in Graphene Oxide Materials on the Reinforcement of Epoxy-Based Nanocomposites," *Journal of Polymer Science Part B-Polymer Physics*, vol. 54, pp. 281-291, Jan 2016.
- [14] C. K. Chua and M. Pumera, "Chemical reduction of graphene oxide: a synthetic chemistry viewpoint," *Chemical Society Reviews*, vol. 43, pp. 291-312, 2014.

- [15] D. R. Cooper, B. D'Anjou, N. Ghattamaneni, B. Harack, M. Hilke, A. Horth, *et al.*, "Experimental review of graphene," *ISRN Condensed Matter Physics*, vol. 2012, 2012.
- [16] A. K. Geim and K. S. Novoselov, "The rise of graphene," *Nature Materials*, vol. 6, pp. 183-191, Mar 2007.
- [17] R. Raccichini, A. Varzi, S. Passerini, and B. Scrosati, "The role of graphene for electrochemical energy storage," *Nature Materials*, vol. 14, pp. 271-279, Mar 2015.
- [18] O. C. Compton and S. T. Nguyen, "Graphene Oxide, Highly Reduced Graphene Oxide, and Graphene: Versatile Building Blocks for Carbon-Based Materials," *Small*, vol. 6, pp. 711-723, Mar 22 2010.
- [19] S. Pei and H.-M. Cheng, "The reduction of graphene oxide," *Carbon*, vol. 50, pp. 3210-3228, Aug 2012.
- [20] W. S. Hummers and R. E. Offeman, "Preperation of Graphitic Oxide," *Journal of the American Chemical Society*, vol. 80, pp. 1339-1339, 1958 1958.
- [21] M. Batzill, "The surface science of graphene: Metal interfaces, CVD synthesis, nanoribbons, chemical modifications, and defects," *Surface Science Reports*, vol. 67, pp. 83-115, Mar 1 2012.
- [22] B. Hu, H. Ago, Y. Ito, K. Kawahara, M. Tsuji, E. Magome, *et al.*, "Epitaxial growth of large-area single-layer graphene over Cu(111)/sapphire by atmospheric pressure CVD," *Carbon*, vol. 50, pp. 57-65, Jan 2012.
- [23] Z. Sun, Z. Liu, J. Li, G.-a. Tai, S.-P. Lau, and F. Yan, "Infrared Photodetectors Based on CVD-Grown Graphene and PbS Quantum Dots with Ultrahigh Responsivity," *Advanced Materials*, vol. 24, pp. 5878-5883, Nov 14 2012.
- [24] B. N. Chandrashekar, B. Deng, A. S. Smitha, Y. Chen, C. Tan, H. Zhang, *et al.*, "Roll-to-Roll Green Transfer of CVD Graphene onto Plastic for a Transparent and Flexible Triboelectric Nanogenerator," *Advanced Materials*, vol. 27, pp. 5210-5216, Sep 16 2015.
- [25] S. Hofmann, P. Braeuninger-Weimer, and R. S. Weatherup, "CVD-Enabled Graphene Manufacture and Technology," *Journal of Physical Chemistry Letters*, vol. 6, pp. 2714-2721, Jul 16 2015.
- [26] V. Miseikis, D. Convertino, N. Mishra, M. Gemmi, T. Mashoff, S. Heun, *et al.*, "Rapid CVD growth of millimetre-sized single crystal graphene using a cold-wall reactor," *2d Materials*, vol. 2, Mar 2015.
- [27] C. Mattevi, H. Kim, and M. Chhowalla, "A review of chemical vapour deposition of graphene on copper," *Journal of Materials Chemistry*, vol. 21, pp. 3324-3334, 2011 2011.
- [28] S. Bae, H. Kim, Y. Lee, X. Xu, J.-S. Park, Y. Zheng, *et al.*, "Roll-to-roll production of 30-inch graphene films for transparent electrodes," *Nature Nanotechnology*, vol. 5, pp. 574-578, Aug 2010.
- [29] T. Kobayashi, M. Bando, N. Kimura, K. Shimizu, K. Kadono, N. Umez, *et al.*, "Production of a 100-m-long high-quality graphene transparent conductive film by roll-to-roll chemical vapor deposition and transfer process," *Applied Physics Letters*, vol. 102, Jan 14 2013.
- [30] E. S. Polsen, D. Q. McNerny, B. Viswanath, S. W. Pattinson, and A. J. Hart, "High-speed roll-to-roll manufacturing of graphene using a concentric tube CVD reactor," *Scientific Reports*, vol. 5, May 21 2015.

- [31] W. S. Koh, C. H. Gan, W. K. Phua, Y. A. Akimov, and P. Bai, "The Potential of Graphene as an ITO Replacement in Organic Solar Cells: An Optical Perspective," *Ieee Journal of Selected Topics in Quantum Electronics*, vol. 20, Jan-Feb 2014.
- [32] W. Cai, R. D. Piner, F. J. Stadermann, S. Park, M. A. Shaibat, Y. Ishii, *et al.*, "Synthesis and solid-state NMR structural characterization of (13)C-labeled graphite oxide," *Science*, vol. 321, pp. 1815-1817, Sep 26 2008.
- [33] T. Szabo, O. Berkesi, and I. Dekany, "DRIFT study of deuterium-exchanged graphite oxide," *Carbon*, vol. 43, pp. 3186-3189, Dec 2005.
- [34] B. C. Brodie, "On the atomic weight of graphite," *Philosophical Transactions of the Royal Society of London*, vol. 149, pp. 249-259, 1859.
- [35] Z. Luo, Y. Lu, L. A. Somers, and A. T. C. Johnson, "High Yield Preparation of Macroscopic Graphene Oxide Membranes," *Journal of the American Chemical Society*, vol. 131, pp. 898+, Jan 28 2009.
- [36] R. Beams, L. G. Cancado, and L. Novotny, "Raman characterization of defects and dopants in graphene," *Journal of Physics-Condensed Matter*, vol. 27, Mar 4 2015.
- [37] B. Qiu, Y. Zhou, Y. Ma, X. Yang, W. Sheng, M. Xing, *et al.*, "Facile synthesis of the Ti3+ self-doped TiO2-graphene nanosheet composites with enhanced photocatalysis," *Scientific reports*, vol. 5, 2015.
- [38] D. Yang, A. Velamakanni, G. Bozoklu, S. Park, M. Stoller, R. D. Piner, *et al.*, "Chemical analysis of graphene oxide films after heat and chemical treatments by X-ray photoelectron and Micro-Raman spectroscopy," *Carbon*, vol. 47, pp. 145-152, Jan 2009.
- [39] S. Park, J. An, J. R. Potts, A. Velamakanni, S. Murali, and R. S. Ruoff, "Hydrazine-reduction of graphite- and graphene oxide," *Carbon*, vol. 49, pp. 3019-3023, Aug 2011.
- [40] A. Lerf, H. Y. He, M. Forster, and J. Klinowski, "Structure of graphite oxide revisited," *Journal of Physical Chemistry B*, vol. 102, pp. 4477-4482, Jun 4 1998.
- [41] K. S. Novoselov, D. Jiang, F. Schedin, T. J. Booth, V. V. Khotkevich, S. V. Morozov, *et al.*, "Two-dimensional atomic crystals," *Proceedings of the National Academy of Sciences of the United States of America*, vol. 102, pp. 10451-10453, Jul 26 2005.
- [42] T. Szabo, O. Berkesi, P. Forgo, K. Josepovits, Y. Sanakis, D. Petridis, *et al.*, "Evolution of surface functional groups in a series of progressively oxidized graphite oxides," *Chemistry of Materials*, vol. 18, pp. 2740-2749, May 30 2006.
- [43] W. Scholz and H. P. Boehm, "Graphite Oxide .6. Structure of Graphite Oxide," *Zeitschrift Fur Anorganische Und Allgemeine Chemie*, vol. 369, pp. 327-&, 1969 1969.
- [44] D. R. Dreyer, A. D. Todd, and C. W. Bielawski, "Harnessing the chemistry of graphene oxide," *Chemical Society Reviews*, vol. 43, pp. 5288-5301, Aug 7 2014.
- [45] T. Nakajima and Y. Matsuo, "FORMATION PROCESS AND STRUCTURE OF GRAPHITE OXIDE," *Carbon*, vol. 32, pp. 469-475, 1994 1994.

- [46] R. J. W. E. Lahaye, H. K. Jeong, C. Y. Park, and Y. H. Lee, "Density functional theory study of graphite oxide for different oxidation levels," *Physical Review B*, vol. 79, p. 125435, 03/27/ 2009.
- [47] D. W. Boukhvalov and M. I. Katsnelson, "Modeling of graphite oxide," *Journal of the American Chemical Society*, vol. 130, pp. 10697-10701, Aug 2008.
- [48] D. W. Boukhvalov and M. I. Katsnelson, "Enhancement of chemical activity in corrugated graphene," *The Journal of Physical Chemistry C*, vol. 113, pp. 14176-14178, 2009.
- [49] J.-A. Yan and M. Y. Chou, "Oxidation functional groups on graphene: Structural and electronic properties," *Physical Review B*, vol. 82, p. 125403, 09/02/ 2010.
- [50] J. T. Paci, T. Belytschko, and G. C. Schatz, "Computational studies of the structure, behavior upon heating, and mechanical properties of graphite oxide," *Journal of Physical Chemistry C*, vol. 111, pp. 18099-18111, Dec 2007.
- [51] Z. Y. Li, W. H. Zhang, Y. Luo, J. L. Yang, and J. G. Hou, "How Graphene Is Cut upon Oxidation?," *Journal of the American Chemical Society*, vol. 131, pp. 6320-+, May 2009.
- [52] R. A. Gaussian 09, G. W. T. M. J. Frisch, H. B. Schlegel, G. E. Scuseria, , J. R. C. M. A. Robb, G. Scalmani, V. Barone, B. Mennucci, , H. N. G. A. Petersson, M. Caricato, X. Li, H. P. Hratchian, , J. B. A. F. Izmaylov, G. Zheng, J. L. Sonnenberg, M. Hada, , K. T. M. Ehara, R. Fukuda, J. Hasegawa, M. Ishida, T. Nakajima, , *et al.*, 2009.
- [53] X. Li and M. J. Frisch, "Energy-represented direct inversion in the iterative subspace within a hybrid geometry optimization method," *Journal of chemical theory and computation*, vol. 2, pp. 835-839, 2006.
- [54] P. Pulay, G. Fogarasi, F. Pang, and J. E. Boggs, "Systematic ab initio gradient calculation of molecular geometries, force constants, and dipole moment derivatives," *Journal of the American Chemical Society*, vol. 101, pp. 2550-2560, 1979.
- [55] G. Fogarasi, X. Zhou, P. W. Taylor, and P. Pulay, "The calculation of ab initio molecular geometries: efficient optimization by natural internal coordinates and empirical correction by offset forces," *Journal of the American Chemical Society*, vol. 114, pp. 8191-8201, 1992.
- [56] P. Pulay and G. Fogarasi, "Geometry optimization in redundant internal coordinates," *The Journal of chemical physics*, vol. 96, pp. 2856-2860, 1992.
- [57] J. Baker, "Techniques for geometry optimization: A comparison of Cartesian and natural internal coordinates," *Journal of computational chemistry*, vol. 14, pp. 1085-1100, 1993.
- [58] C. Peng and H. Bernhard Schlegel, "Combining Synchronous Transit and Quasi- Newton Methods to Find Transition States," *Israel Journal of Chemistry*, vol. 33, pp. 449-454, 1993.
- [59] C. Peng, P. Y. Ayala, H. B. Schlegel, and M. J. Frisch, "Using redundant internal coordinates to optimize equilibrium geometries and transition states," *Journal of Computational Chemistry*, vol. 17, pp. 49-56, 1996.
- [60] J. Paier, R. Hirschl, M. Marsman, and G. Kresse, "The Perdew–Burke–Ernzerhof exchange-correlation functional applied to the G2-1 test set using a plane-wave basis set," *The Journal of chemical physics*, vol. 122, p. 234102, 2005.



- [61] W. Kohn and L. J. Sham, "Self-Consistent Equations Including Exchange and Correlation Effects," *Physical Review*, vol. 140, pp. A1133-A1138, 11/15/ 1965.
- [62] K. Schwarz and P. Blaha, "Solid state calculations using WIEN2k," *Computational Materials Science*, vol. 28, pp. 259-273, Oct 2003.
- [63] K. Schwarz, P. Blaha, and S. B. Trickey, "Electronic structure of solids with WIEN2k," *Molecular Physics*, vol. 108, pp. 3147-3166, 2010 2010.
- [64] H. J. Monkhorst and J. D. Pack, "Special points for Brillouin-zone integrations," *Physical Review B*, vol. 13, pp. 5188-5192, 06/15/ 1976.
- [65] A. Hunt, D. A. Dikin, E. Z. Kurmaev, Y. H. Lee, N. V. Luan, G. S. Chang, *et al.*, "Modulation of the band gap of graphene oxide: The role of AA-stacking," *Carbon*, vol. 66, pp. 539-546, 1// 2014.
- [66] D. D'Angelo, C. Bongiorno, M. Amato, I. Deretzis, A. La Magna, G. Compagnini, *et al.*, "Electron energy-loss spectra of graphene oxide for the determination of oxygen functionalities," *Carbon*, vol. 93, pp. 1034-1041, 11// 2015.
- [67] D. W. Boukhvalov, "DFT modeling of the covalent functionalization of graphene: from ideal to realistic models," *Rsc Advances*, vol. 3, pp. 7150-7159, 2013.
- [68] R. Mortezaee, "Computational Modeling of Graphene Oxide Exfoliation and Lithium Storage Characteristics," 2013.
- [69] N. Lu, Y. Huang, H.-b. Li, Z. Li, and J. Yang, "First principles nuclear magnetic resonance signatures of graphene oxide," *The Journal of Chemical Physics*, vol. 133, p. 034502, 2010.
- [70] J. O. Sofo, A. S. Chaudhari, and G. D. Barber, "Graphane: A two-dimensional hydrocarbon," *Physical Review B*, vol. 75, p. 153401, 04/10/ 2007.
- [71] S. Kim, S. Zhou, Y. Hu, M. Acik, Y. J. Chabal, C. Berger, *et al.*, "Room-temperature metastability of multilayer graphene oxide films," *Nat Mater*, vol. 11, pp. 544-549, 06//print 2012.
- [72] G. Lee and K. Cho, "Electronic structures of zigzag graphene nanoribbons with edge hydrogenation and oxidation," *Physical Review B*, vol. 79, p. 165440, 04/29/ 2009.
- [73] W. Gao, L. B. Alemany, L. Ci, and P. M. Ajayan, "New insights into the structure and reduction of graphite oxide," *Nat Chem*, vol. 1, pp. 403-408, 08//print 2009.
- [74] W. W. Cai, R. D. Piner, F. J. Stadermann, S. Park, M. A. Shaibat, Y. Ishii, *et al.*, "Synthesis and solid-state NMR structural characterization of (13)C-labeled graphite oxide," *Science*, vol. 321, pp. 1815-1817, Sep 2008.
- [75] Z. Li, W. Zhang, Y. Luo, J. Yang, and J. G. Hou, "How graphene is cut upon oxidation?," *Journal of the American Chemical Society*, vol. 131, pp. 6320-6321, 2009.
- [76] L. Wang, Y. Sun, K. Lee, D. West, Z. Chen, J. Zhao, *et al.*, "Stability of graphene oxide phases from first-principles calculations," *Physical Review B*, vol. 82, p. 161406, 2010.
- [77] F. A. Carey and R. J. Sundberg, *Advanced Organic Chemistry: Part A: Structure and Mechanisms*: Springer Science & Business Media, 2007.
- [78] G. A. Jeffrey and G. A. Jeffrey, *An introduction to hydrogen bonding* vol. 12: Oxford university press New York, 1997.

- [79] D. C. Marcano, D. V. Kosynkin, J. M. Berlin, A. Sinitskii, Z. Sun, A. Slesarev, *et al.*, "Improved synthesis of graphene oxide," *ACS nano*, vol. 4, pp. 4806-4814, 2010.
- [80] X. Gao, J. Jang, and S. Nagase, "Hydrazine and thermal reduction of graphene oxide: reaction mechanisms, product structures, and reaction design," *The Journal of Physical Chemistry C*, vol. 114, pp. 832-842, 2009.
- [81] C. Gómez-Navarro, R. T. Weitz, A. M. Bittner, M. Scolari, A. Mews, M. Burghard, *et al.*, "Electronic transport properties of individual chemically reduced graphene oxide sheets," *Nano Letters*, vol. 9, pp. 2206-2206, 2009.
- [82] G. Eda, C. Mattevi, H. Yamaguchi, H. Kim, and M. Chhowalla, "Insulator to semimetal transition in graphene oxide," *The Journal of Physical Chemistry C*, vol. 113, pp. 15768-15771, 2009.
- [83] E. C. Mattson, H. Pu, S. Cui, M. A. Schofield, S. Rhim, G. Lu, *et al.*, "Evidence of nanocrystalline semiconducting graphene monoxide during thermal reduction of graphene oxide in vacuum," *ACS nano*, vol. 5, pp. 9710-9717, 2011.
- [84] A. Mathkar, D. Tozier, P. Cox, P. Ong, C. Galande, K. Balakrishnan, *et al.*, "Controlled, stepwise reduction and band gap manipulation of graphene oxide," *The journal of physical chemistry letters*, vol. 3, pp. 986-991, 2012.
- [85] M. A. Velasco-Soto, S. A. Pérez-García, J. Alvarez-Quintana, Y. Cao, L. Nyborg, and L. Licea-Jiménez, "Selective band gap manipulation of graphene oxide by its reduction with mild reagents," *Carbon*, vol. 93, pp. 967-973, 11// 2015.
- [86] J. Chen, Y. Zhang, M. Zhang, B. Yao, Y. Li, L. Huang, *et al.*, "Water-enhanced oxidation of graphite to graphene oxide with controlled species of oxygenated groups," *Chemical Science*, vol. 7, pp. 1874-1881, 2016.
- [87] J. P. Rourke, P. A. Pandey, J. J. Moore, M. Bates, I. A. Kinloch, R. J. Young, *et al.*, "The Real Graphene Oxide Revealed: Stripping the Oxidative Debris from the Graphene-like Sheets," *Angewandte Chemie-International Edition*, vol. 50, pp. 3173-3177, 2011 2011.
- [88] Y. Zhu, S. Murali, W. Cai, X. Li, J. W. Suk, J. R. Potts, *et al.*, "Graphene and Graphene Oxide: Synthesis, Properties, and Applications," *Advanced Materials*, vol. 22, pp. 3906-3924, Sep 15 2010.
- [89] K. S. Choi, Y. Park, K.-C. Kwon, J. Kim, C. K. Kim, S. Y. Kim, *et al.*, "Reduced graphite oxide-indium tin oxide hybrid materials for use as a transparent electrode," *Journal of The Electrochemical Society*, vol. 158, pp. J231-J235, 2011.
- [90] H. Yang, T. Song, S. Lee, H. Han, F. Xia, A. Devadoss, *et al.*, "Tin indium oxide/graphene nanosheet nanocomposite as an anode material for lithium ion batteries with enhanced lithium storage capacity and rate capability," *Electrochimica Acta*, vol. 91, pp. 275-281, 2013.
- [91] J. Liu, Y. Yi, Y. Zhou, and H. Cai, "Highly stretchable and flexible graphene/ITO hybrid transparent electrode," *Nanoscale research letters*, vol. 11, p. 108, 2016.

## APPENDIX 1

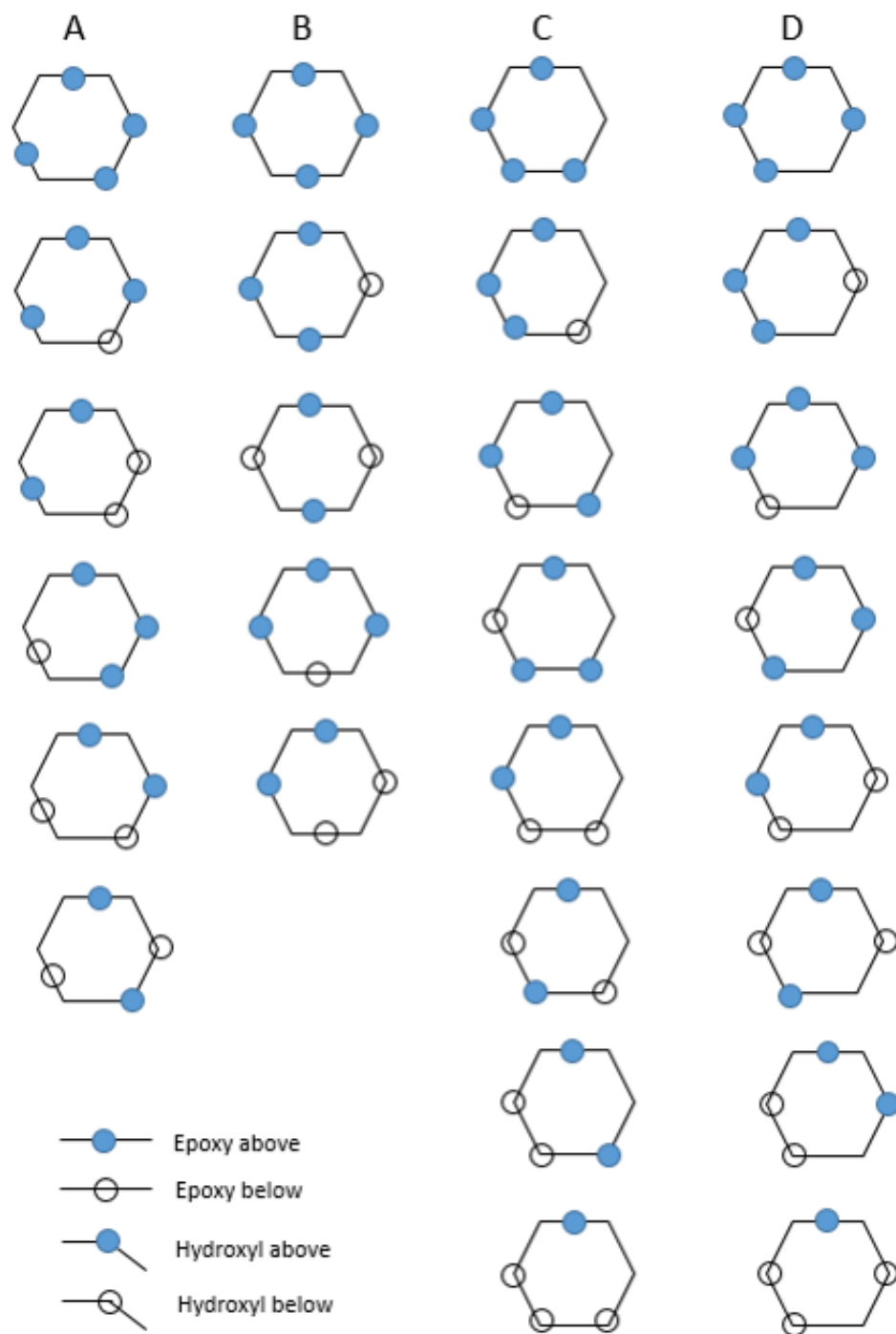


Figure A1 Schematic  $C_6O_4$  isomer models: Type A: 1, 3-epoxy substituted  $C_6O_2(OH)_2$ ; Type B: 1, 4-epoxy substituted  $C_6O_2(OH)_2$ ; Type C: 1, 2, 3-hydroxyl substituted  $C_6O_1(OH)_3$ ; Type D: 1, 2, 4-hydroxyl substituted  $C_6O_1(OH)_3$ .

This poster is published on the 24th Australian Conference on Microscopy and Microanalysis 2016.



## A Theoretical Study of Graphene Oxide

Haining Luo<sup>1</sup>, Graeme John Auchterlonie<sup>2</sup>, Jin Zou<sup>1,2</sup>

<sup>1</sup>School of Mechanical and Mining Engineering, <sup>2</sup>Centre for Microscopy & Microanalysis, The University of Queensland, 4072, Brisbane, Queensland, Australia. Corresponding author: G.Auchterlonie@uq.edu.au

### Introduction

Graphene Oxide (GO) is a two-dimensional atomic carbon sheet bearing oxygen or oxidative debris on its basal planes [1]. It is one of the source materials for large quantity graphene production and has potential in flexible organic photovoltaic cells and Li-ion batteries [2]. People have suggested different structural models for GO, but the precise chemical structure of GO is still controversial. Major reasons include sample-to-sample variability due to different synthesis methods, the degree of oxidation, the amorphous and nonstoichiometric nature of GO, as well as limited resolution in the major characterization techniques such as SSNMR and FTIR [3]. Beyond these difficulties, functionalization and reduction of GO can be more precisely determined, to reveal the real model of GO structure and enable reliable production.

### Method

The new GO model is based on an classic model proposed by Lerf-Klinowski (LK Model) [4]. The LK model is mostly accepted by the world because its consistence with the experiment observation. In LK model, Lerf and co-workers proposed that epoxide groups and hydroxyl groups are attached to the GO plane randomly while the ketone groups are more favoured at the periphery of GO than carboxylic acids. But due to the complexity on the GO local environment, such as the steric effect of epoxy and hydroxyl groups, were not sufficiently considered. Moreover, new GO models with C/O ratio of 1.5:1 (Nominal Composition of commercially available GO such as products from Graphenea® and ACS MATERIAL®) are built and calculated in a computer software program, ChemBio3D [5]. In ChemBio3D, GO molecule can be modeled by molecular mechanics using force field which can calculate the potential energy of the system. The MM2 force field method developed by Allinger [6] is a classical force field used for calculating properties of organic molecular models. It is designed to reproduce the equilibrium covalent geometry of molecules as precisely as possible [6]. By comparing the steric energy of isomeric GO model, we can find the relative positions of epoxy and hydroxyl groups which then calculate the most stable structure. However, the limited computing power of the program is unable to calculate models for large numbers of atoms. The tables below show the current results of these calculations.

Table 1  $C_{24}O_4$  cell model and calculation results

Chemical formula	Structure	Unit Model	Energy minimization	Steric Energy (kcal/mol)
$C_{24}O_4$ -a				27.4502
$C_{24}O_4$ -b				20.8932
$C_{24}O_4$ -c				47.6480
$C_{24}O_4$ -d				21.6712


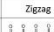

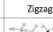









Table 2  $C_{24}O_{16}$  cell model and calculation results

Chemical formula	Structure	Unit Cell	Energy minimization	Steric Energy (kcal/mol)
$C_{24}O_{16}$ -a				2245.1266
$C_{24}O_{16}$ -b				1854.6090
$C_{24}O_{16}$ -c				2222.8868
$C_{24}O_{16}$ -d				2003.0864

Table 3  $C_{24}O_{36}$  cell model and calculation results

Chemical formula	Structure	Unit Cell	Energy minimization	Steric Energy (kcal/mol)
$C_{24}O_{36}$ -a				3747.0033
$C_{24}O_{36}$ -b				3465.2756
$C_{24}O_{36}$ -c				3794.7067
$C_{24}O_{36}$ -d				3913.0733

Table 4 GO edge model and calculation results

Function group			-COOH		-OH	
Orientation	Zigzag	Armchair	Zigzag	Armchair	Zigzag	Armchair
Structure						
Energy minimization						
Steric Energy (kcal/mol)	26.5281	52.8723	26.4628	0.6027	26.4628	26.8975

### Results

According to the chemical composition, the basic benzene-like GO model contains 6 carbon atoms and 4 oxygen atoms. There are 4 different isomers of the  $C_6O_4$  cell listed in the table. The  $C_{24}O_{16}$  and  $C_{24}O_{36}$  supercells are both derived from the basic  $C_6O_4$  cell. Limited by the calculation complexity, the maximum number of carbon atoms in a single model is 54. Through the energy minimization calculation, the steric energy of each isomers can be compared and the lowest one be selected as the preferred structure. From Table 1 to Table 3, the b-type model with para-substituted epoxide is the most stable structure.

The edge structure is simplified to a 4x4 graphene supercell with only one side decorated by ketone, carbonyl and hydroxyl group. The steric energy shows the preferred orientation of the edge functional group. The armchair-carbonyl has the lowest steric energy while the armchair-ketone has the highest steric energy.

### Conclusion

A new structure for GO has been described which has the chemical formula  $C_{1.5}O:H$  and fits many experimentally determined parameters [7]. This model is shown schematically in Figure 5.1 and includes two regions: The first, graphene-like area with benzene rings and oxidized region (in red) with surface bounded oxygen debris. Two functional groups exist in each GO cells, that is, para-substituted epoxide groups with interspersed hydroxyl groups on two sides of the GO plane. The size of the debris depends mainly on the oxidation level of GO. The second, on the edge of GO sheet, the carbonyl prefer attachment along the armchair orientation, while the ketones prefer attachment in the zigzag direction.

The carbon grid has a moderate wrinkling due to the oxygen debris. This deformation is located around hydroxyl and epoxide molecules where the  $sp^3$  hybridization is induced in C-C bonds. Despite the deformation, GO still maintains a hexagonal graphene-like structure. This structure stability results from the transfiguration arrangement of the hydroxyl and epoxide oxygen.

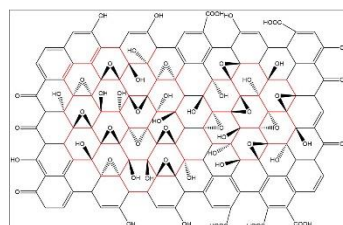


Figure 1 New structure model of GO; Red zones represent the oxidized area.

### References

- [1] D. A. Dikin, S. Stankovich, E. J. Zimney, R. D. Piner, G. H. B. Dommett, G. Evmenenko, et al., "Preparation and characterization of graphene oxide paper," *Nature*, vol. 448, pp. 457-460, 2007.
- [2] R. Mortezaei, "Computational Modeling of Graphene Oxide Exfoliation and Lithium Storage Characteristics," 2013.
- [3] L. B. Casablancas, M. A. Shalbat, W. W. Cai, S. Park, R. Piner, R. S. Ruoff, and Y. Ichii, "NMR-Based Structural Modeling of Graphite Oxide Using Multidimensional 2D Solid-State NMR and ab initio Chemical Shift Calculations," *Journal of the American Chemical Society*, 2010, 132(15) p. 5672-5676.
- [4] A. Lerf, H. Y. He, M. Forster, and I. Klinowski, "Structure of graphite oxide revisited," *Journal of Physical Chemistry B*, vol. 102, pp. 4477-4482, Jun 4 1998.
- [5] R. Pohl, "Software Review: ChemBioDraw Ultra 11.01 for Mac," *Chemistry in Australia*, vol. 75, p. 28, 2008.
- [6] N. L. Allinger, "Conformational analysis. 130. MM2: A hydrocarbon force field utilizing V1 and V2 torsional terms," *Journal of the American Chemical Society*, vol. 99, pp. 8127-8134, 1977.
- [7] H. A. Becerril, J. Mao, Z. Liu, R. M. Stoltenberg, Z. Bao, and Y. Chen, "Evaluation of solution-processed reduced graphene oxide films as transparent conductors," *ACS Nano*, 2008, 2(5) p. 463-470.